

Investigating the two-pion exchange of the double charm DD^* chiral interactions and T_{cc}

Hao Xu^{1*} and Li-Xiang Ren^{1†}

¹*Institute of Theoretical Physics, College of Physics and Electronic Engineering,
Northwest Normal University, Lanzhou 730070, China*

Under chiral effective field theory, we study the S -wave DD^* interactions up to second chiral order at one-loop level, which contain full contact, one-pion-exchange (OPE) and two-pion-exchange (TPE) contributions. Here, we adopt a new subtraction scheme of the two-particle-reducible contributions, and introduce three regularization schemes uniquely for the TPE contributions since they are highly divergent on the momentum transfer. These different schemes all lead to same conclusions: In the $I=0$ channel, the TPE contribution is repulsive, then the competition between this powerful repulsing TPE and the other two (contact and OPE) results in a quite weak attraction. This explains why T_{cc} has a extremely small binding energy if treated as the $I = 0$ DD^* bound state. This feature resembles that of hidden charm DD^* as we investigated in previous work [1], which also interpreted the extremely near-threshold phenomenon of $X(3872)$. In addition, we also solve the Bethe-Salpeter equation with the chiral interactions for a consistency check.

I. INTRODUCTION

The elaborate study of the heavy hadron interactions is a crucial aspect in the nonperturbative QCD physics. It helps us to uncover the interacting mechanism of low energy QCD where the fundamental quarks and gluons have been confined, and can also be directly utilized to understand the heavy exotic states and near-threshold phenomena, even served as a nonperturbative QCD input to other areas. The advantage in the heavy hadron sector is that the emergent symmetry, i.e. the heavy quark symmetry, can be applied to benefit our studies.

There has been many kinds of methods to deal with the heavy hadron interactions and related exotic states. For example, the one-boson-exchange (OBE) model is one of the appropriate dynamical models. This model constructs effective meson interactions by taking into account various meson exchanges (π , σ , ρ , ω meson and etc). For example, Ref. [2] successfully applied the OBE model to the $D\bar{D}^*$ and $X(3872)$ study. See Ref. [3] for details about the OBE model. Other hadron-level approaches have also been widely used such as the contact-range method, local hidden gauge approach, non-relativistic effective field theory and other effective lagrangian approaches [4–8]. There also exists quark-level approaches, where the interactions and concerned multi-quark systems are evaluated based on the quark model [9–12]. In addition, lattice studies play an indispensable role in the area [13, 14]. We also refer to Refs. [15–22] for other approaches not mentioned. Among them, chiral field effective theory (ChEFT) is one of the promising frameworks dealing with the heavy hadron interactions, which will be adopted in this work.

ChEFT was originally proposed to deal with the nucleon-nucleon interaction [23, 24], it has been fully developed in last decades and gives us a deep understanding of the nuclear force [25–31]. Similar to chiral perturbation theory [32], ChEFT framework respects the chiral symmetry and arranges the low energy nucleon-nucleon interaction in a systematic way, so that the interaction is classified as direct contact

and multi-Goldstone exchange contributions. Here unique schemes such as Weinberg scheme have to be applied to keep a correct power counting. In Weinberg scheme [23, 24], with the standard power-counting rule one calculates the two-particle-irreducible (2PI) diagrams, i.e. the effective potential, then iterates it into the equation (e.g. the Schrödinger or Lippmann-Schwinger equation) to retrieve rest two-particle-reducible (2PR) contributions.

In a word, two advantages of ChEFT are prominent: the interaction is dealt with in a systematic way, and it manifests as the multi-Goldstone exchanges. So it is promising to apply ChEFT to the heavy hadron interactions. In the heavy hadron sector, ChEFT adopting Weinberg scheme has indeed been developed in recent years. In Ref. [33], the authors introduced the ChEFT framework to study the doubly-bottomed system $\bar{B}\bar{B}$ up to next-to-leading order (NLO), especially they analyzed the two-pion-exchange contributions in detail. Based on this Pioneer work [33], the authors in Ref. [34] developed the framework and applied the ChEFT to the doubly-charmed DD^* system. A molecular state in the $I = 0$ channel was predicted then, which just matched the T_{cc}^+ state discovered later. The author in Ref. [1] extended to the hidden-charm DD^* system by considering the proper charge conjugation properties of the heavy hadrons. The authors in Ref. [35] systematically studied the $D^{(*)}\bar{B}^{(*)}$ systems and their coupled-channel effects. Following this framework, other two-heavy hadron systems were also studied [31, 36–45].

Follow our previous work [34], we continue to investigate the DD^* interactions. DD^* is a typical two heavy hadron system and similar to NN , due to their same isospin configurations and similar interactions with the Goldstone bosons, so we can draw lessons from the researches in the NN sector. Furthermore, because of the additional symmetry, i.e. heavy quark symmetry, the interactions in the heavy hadron sector can be simplified to a good approximation. Specifically, in this work the heavy hadron formalism will be adopted. Therefore, the study of the DD^* interactions can surely help us to reveal the non-perturbative QCD dynamics. On the other hand, due to the observation of T_{cc} in recent years [46, 47], the related DD^* interactions are now surely under the spotlight.

In 2021, T_{cc}^+ was observed by the LHCb collaboration in the distribution of the $D^0D^0\pi^+$ invariant mass [46, 47], its mass

* xuh2020@nwnu.edu.cn

† 2023212235@nwnu.edu.cn

difference referring to the $D^0 D^{*+}$ threshold is only around 300 keV. Its extremely near-threshold nature as well as the exotic $cc\bar{u}\bar{d}$ content implicate T_{cc}^+ is a possible DD^* molecular candidate. In theory, T_{cc} and the DD^* system have been also studied in various models, such as the molecular approaches [7, 48–57], quark-level approaches [58–64], lattice simulations [65–75], as well as the production mechanisms [76–79].

So in this work we will study the DD^* interactions within ChEFT. Besides our earlier work mentioned above [34], there has been other works discussing the DD^* interactions and T_{cc}^+ under ChEFT recently. The authors in Ref. [80] revisited the DD^* chiral interactions of Ref. [34] by introducing the local momentum-space regularization. The authors in Ref. [81] investigated the two-pion-exchange contributions in a general formalism (without the heavy hadron approach). Despite not DD^* , authors in Ref. [82] studied the two-pion exchange of the $B^{(*)}B^{(*)}$ and $B^{(*)}\bar{B}^{(*)}$ systems, where the coupled channels were taken into account.

In this research, we study the DD^* chiral interactions under ChEFT within heavy hadron formalism, up to NLO at one-loop level, where Weinberg scheme is adopted. Confronting previous work [34], here we will further correct the defect of the previous 2PR subtraction method, and elaborately explore the regularization schemes uniquely for the two-pion exchange because of the intrinsic difficulty it faces. We also solve the Bethe-Salpeter (BS) equation to explore the consistency between different iterative equations. Actually Main conclusions do not change with our new results, but new insights about the DD^* binding force and the T_{cc} state appear.

This paper is organized as follows. In Sec. II we briefly review the chiral interactions of the concerned DD^* system, express the calculated potentials of the individual contact, one-pion-exchange (OPE) and two-pion-exchange (TPE) contributions, then discuss the 2PR reduction scheme and the regularization of the potentials especially for the TPE. In Sec. III, we present the numerical results along with an elaborate discussion of the TPE contributions under different schemes. In Sec. IV, we iterate the DD^* chiral interactions into the BS equation for comparing. The last section is the summary.

II. THE CHIRAL INTERACTIONS OF THE DD^* SYSTEM

Following the Refs. [1, 33, 34], we continue to investigate the DD^* interactions under ChEFT. This framework arranges the amplitudes with an expansion parameter $\epsilon = p/\Lambda_\chi$ (p stands for a small momentum, pion mass, or $D-D^*$ mass splitting). Specifically, we will construct the Lagrangians and interaction potentials by the order parameter ϵ with Weinberg's power counting scheme [23, 24]. Note that in this work the flavor $SU(2)$ symmetry is adopted.

A. The chiral Lagrangians

As in Ref. [34], we will calculate the amplitudes or interaction potentials up to second order $O(\epsilon^2)$ at one-loop level,

so the $D^{(*)}D^{(*)}\pi$ Lagrangian and $4D^{(*)}$ contact Lagrangian at leading order are needed.

Under the flavor $SU(2)$ symmetry, the $DD^*\pi$ lagrangian at $O(\epsilon^1)$ reads [83–85]:

$$\begin{aligned} \mathcal{L}_{H\phi}^{(1)} = & -\langle (i\nu \cdot \partial H)\bar{H} \rangle + \langle H\nu \cdot \Gamma\bar{H} \rangle + g\langle H\nu\gamma_5\bar{H} \rangle \\ & -\frac{1}{8}\delta\langle H\sigma^{\mu\nu}\bar{H}\sigma_{\mu\nu} \rangle, \end{aligned} \quad (1)$$

with the axial vector field $u_\mu = \frac{i}{2}\{\xi^\dagger, \partial_\mu\xi\}$ and chiral connection $\Gamma_\mu = \frac{i}{2}[\xi^\dagger, \partial_\mu\xi]$, where $\xi = \exp(i\phi/2f)$ with

$$\phi = \sqrt{2} \begin{pmatrix} \frac{\pi^0}{\sqrt{2}} & \pi^+ \\ \pi^- & -\frac{\pi^0}{\sqrt{2}} \end{pmatrix}. \quad (2)$$

The (D, D^*) doublet H is

$$\begin{aligned} H &= \frac{1+\not{v}}{2} (P_\mu^* \gamma^\mu + iP\gamma_5), \\ \bar{H} &= \gamma^0 H^\dagger \gamma^0 = (P_\mu^{\dagger*} \gamma^\mu + iP^\dagger \gamma_5) \frac{1+\not{v}}{2}, \\ P &= (D^0, D^+), \quad P_\mu^* = (D^{*0}, D^{*+})_\mu. \end{aligned} \quad (3)$$

The contact Lagrangian at $O(\epsilon^0)$ is also needed [4, 33, 86]:

$$\begin{aligned} \mathcal{L}_{4H}^{(0)} = & D_a \text{Tr}[H\gamma_\mu\bar{H}]\text{Tr}[H\gamma^\mu\bar{H}] \\ & + D_b \text{Tr}[H\gamma_\mu\gamma_5\bar{H}]\text{Tr}[H\gamma^\mu\gamma_5\bar{H}] \\ & + E_a \text{Tr}[H\gamma_\mu\tau^a\bar{H}]\text{Tr}[H\gamma^\mu\tau_a\bar{H}] \\ & + E_b \text{Tr}[H\gamma_\mu\gamma_5\tau^a\bar{H}]\text{Tr}[H\gamma^\mu\gamma_5\tau_a\bar{H}], \end{aligned} \quad (4)$$

where the low energy constants (LECs) D_a, D_b, E_a, E_b should be determined by other methods. The Lagrangians at $O(\epsilon^2)$, which are needed to renormalize the $O(\epsilon^2)$ loop amplitudes, can be found in Refs. [33, 34].

The adopted Weinberg's power counting scheme [23, 24] tells us that, with the chiral power counting we calculate the sum of the two-particle-irreducible (2PI) diagrams first, then iterate it into the Schrödinger, Lippmann-Schwinger or BS equation, where the two-particle-reducible (2PR) contributions can be restored. Here we will calculate the interaction potentials then solve the Schrödinger equation.

B. The diagrams of the DD^* scattering and the DD^* interaction potentials

The flavor wave functions $|I; K\rangle$ of the DD^* system with isospin $I = 0, 1$ and momentum K can be written as

$$\begin{aligned} |0, 0; K\rangle &= \frac{1}{\sqrt{2}} (|D^0 D^{*+}\rangle - |D^+ D^{*0}\rangle), \\ |1, 0; K\rangle &= \frac{1}{\sqrt{2}} (|D^0 D^{*+}\rangle + |D^+ D^{*0}\rangle), \\ |1, 1; K\rangle &= |D^+ D^{*+}\rangle, \\ |1, -1; K\rangle &= |D^0 D^{*0}\rangle. \end{aligned} \quad (5)$$

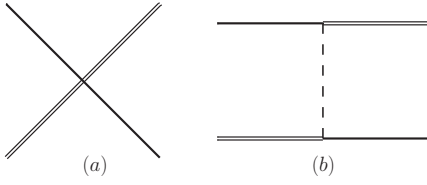


FIG. 1. Tree-level diagrams of the DD^* system at $O(\epsilon^0)$. The solid, double-solid, and dashed lines stand for D , D^* , and π , respectively.

Considering the above flavor wave functions, we can calculate interaction potentials $\mathcal{V}^{l=0,1}$ up to the chiral order $O(\epsilon^2)$ at one-loop level (NLO). just at this order, the non-trivial TPE contribution emerges.

We now show the calculated potentials containing all the 2PI contributions. At $O(\epsilon^0)$ (tree-level), there exists a OPE and a contact 2PI diagram which are showing in Fig. 1. With the help of the Lagrangians (1) and (4) we obtain their contributions to $\mathcal{V}^{l=0,1}$:

$$\mathcal{V}_{\text{contact}(0)}^{l=0} = 2(D_a + D_b - 3E_a - 3E_b)\varepsilon \cdot \varepsilon^*, \quad (6)$$

$$\mathcal{V}_{\text{contact}(0)}^{l=1} = 2(D_a - D_b + E_a - E_b)\varepsilon \cdot \varepsilon^*, \quad (7)$$

$$\mathcal{V}_{1\pi(0)}^{l=0} = \frac{3}{4} \frac{g^2}{f^2} \frac{1}{q^2 - m^2} q \cdot \varepsilon q \cdot \varepsilon^*, \quad (8)$$

$$\mathcal{V}_{1\pi(0)}^{l=1} = \frac{1}{4} \frac{g^2}{f^2} \frac{1}{q^2 - m^2} q \cdot \varepsilon q \cdot \varepsilon^*. \quad (9)$$

In the above expressions, the subscript (0) of \mathcal{V} stands for the order $O(\epsilon^0)$, q denotes the momentum transfer between initial and final states, and m , m_1 and m_2 are the masses of π , D and D^* respectively. In addition, ε and ε^* are the polarization vectors.

For the diagrams at $O(\epsilon^2)$, there appears 1-loop TPE diagrams, as well as 1-loop corrections to the $O(\epsilon^0)$ contact and OPE diagrams, which are showing in Figs. 2 and 3. As in Ref. [34] we ignore the finite parts of the $O(\epsilon^2)$ tree-level amplitudes here due to the lack of their LEC informations, of course their divergent parts are used to renormalize the $O(\epsilon^2)$ 1-loop diagrams [34]. According to Figs. 2 and 3 we now show the calculated \mathcal{V} at $O(\epsilon^2)$ as individual contact, OPE and TPE contributions:

$$\begin{aligned} \mathcal{V}_{\text{contact}(2)}^{l=0} = & \frac{3g^2}{2f^2} \left\{ -C_1(d-1)\partial_\omega J_{22}^b(-\delta) - C_1(d-2)\partial_\omega J_{22}^b(0) - C_1\partial_\omega J_{22}^b(\delta) - C_1 J_{22}^h(-\delta, \delta) - C_1 J_{22}^h(\delta, -\delta) \right. \\ & - (dC_2 + 2C_4)J_{22}^g(-\delta, -\delta) - C_2(d-3)(d-2)J_{22}^g(0, 0) - 2C_3J_{22}^g(\delta, \delta) - 2C_4J_{22}^g(-\delta, \delta) - 2C_4J_{22}^g(\delta, -\delta) \\ & \left. - 2C_5(d-3)(d-2)J_{22}^h(0, -\delta) - 2C_5(d-3)(d-2)J_{22}^h(-\delta, 0) \right\} \varepsilon \cdot \varepsilon^*, \end{aligned} \quad (10)$$

$$\begin{aligned} \mathcal{V}_{\text{contact}(2)}^{l=1} = & \frac{g^2}{2f^2} \left\{ -3C_2(d-1)\partial_\omega J_{22}^b(-\delta) - 3C_2(d-2)\partial_\omega J_{22}^b(0) + 3(C_4 - C_3)\partial_\omega J_{22}^b(\delta) + (C_4 - C_3)J_{22}^h(-\delta, \delta) \right. \\ & + (C_4 - C_3)J_{22}^h(\delta, -\delta) - 4C_3J_{22}^g(\delta, \delta) + 4C_4J_{22}^g(-\delta, \delta) + 4C_4J_{22}^g(\delta, -\delta) - 2C_5(d-3)(d-2)J_{22}^g(0, -\delta) \\ & - 2C_5(d-3)(d-2)J_{22}^g(-\delta, 0) + \left[(2-3d)D_a + (d-2)D_b + (d-6)E_a + 5(d-2)E_b \right] J_{22}^g(-\delta, -\delta) \\ & \left. - (d-3)(d-2)(3D_a - D_b - E_a - 5E_b)J_{22}^g(0, 0) \right\} \varepsilon \cdot \varepsilon^*, \end{aligned} \quad (11)$$

$$\begin{aligned} \mathcal{V}_{1\pi(2)}^{l=0} = & \frac{-3}{16f^4} \frac{1}{p^2 - m^2} \left\{ g^4 \left[3(d-1)\partial_\omega J_{22}^b(-\delta) + 3(d-2)\partial_\omega J_{22}^b(0) + 3\partial_\omega J_{22}^b(\delta) + (d-3)(d-2)J_{22}^g(0, -\delta) \right. \right. \\ & \left. \left. + (d-3)(d-2)J_{22}^g(-\delta, 0) - J_{22}^g(-\delta, \delta) - J_{22}^g(\delta, -\delta) \right] - 8g^2 J_0^c \right\} q \cdot \varepsilon q \cdot \varepsilon^*, \end{aligned} \quad (12)$$

$$\begin{aligned} \mathcal{V}_{1\pi(2)}^{l=1} = & \frac{-1}{16f^4} \frac{1}{p^2 - m^2} \left\{ g^4 \left[3(d-1)\partial_\omega J_{22}^b(-\delta) + 3(d-2)\partial_\omega J_{22}^b(0) + 3\partial_\omega J_{22}^b(\delta) + (d-3)(d-2)J_{22}^g(0, -\delta) \right. \right. \\ & \left. \left. + (d-3)(d-2)J_{22}^g(-\delta, 0) - J_{22}^g(-\delta, \delta) - J_{22}^g(\delta, -\delta) \right] - 8g^2 J_0^c \right\} q \cdot \varepsilon q \cdot \varepsilon^*, \end{aligned} \quad (13)$$

$$\begin{aligned} \mathcal{V}_{2\pi(2)}^{l=0} = & \frac{3}{16f^4} \left\{ \left[-3(d-3)J_{22}^B(-\delta, 0)\vec{q}^4 + (d-3)J_{22}^R(-\delta, 0)\vec{q}^4 - 6(d-3)J_{32}^B(-\delta, 0)\vec{q}^4 + 2(d-3)J_{32}^R(-\delta, 0)\vec{q}^4 \right. \right. \\ & - 3(d-3)J_{43}^B(-\delta, 0)\vec{q}^4 + (d-3)J_{43}^R(-\delta, 0)\vec{q}^4 + 6(d-3)J_{21}^B(-\delta, 0)\vec{q}^2 - (d-3)J_{21}^R(-\delta, 0)\vec{q}^2 + (d-3)J_{21}^B(-\delta, -\delta)\vec{q}^2 \\ & + 3(d-3)(2d+1)J_{31}^B(-\delta, 0)\vec{q}^2 + 3J_{31}^B(-\delta, \delta)\vec{q}^2 - (d-3)(2d+1)J_{31}^R(-\delta, 0)\vec{q}^2 - J_{31}^R(-\delta, \delta)\vec{q}^2 \\ & + 3(d-3)(2d+1)J_{42}^B(-\delta, 0)\vec{q}^2 + 3J_{42}^B(-\delta, \delta)\vec{q}^2 - (d-3)(2d+1)J_{42}^R(-\delta, 0)\vec{q}^2 - J_{42}^R(-\delta, \delta)\vec{q}^2 \\ & \left. \left. - 3(d-3)(d-2)(d+1)J_{41}^B(-\delta, 0) - 3(d+1)J_{41}^B(-\delta, \delta) + (d-3)(d-2)(d+1)J_{41}^R(-\delta, 0) + (d+1)J_{41}^R(-\delta, \delta) \right] g^4 \right\} \end{aligned}$$

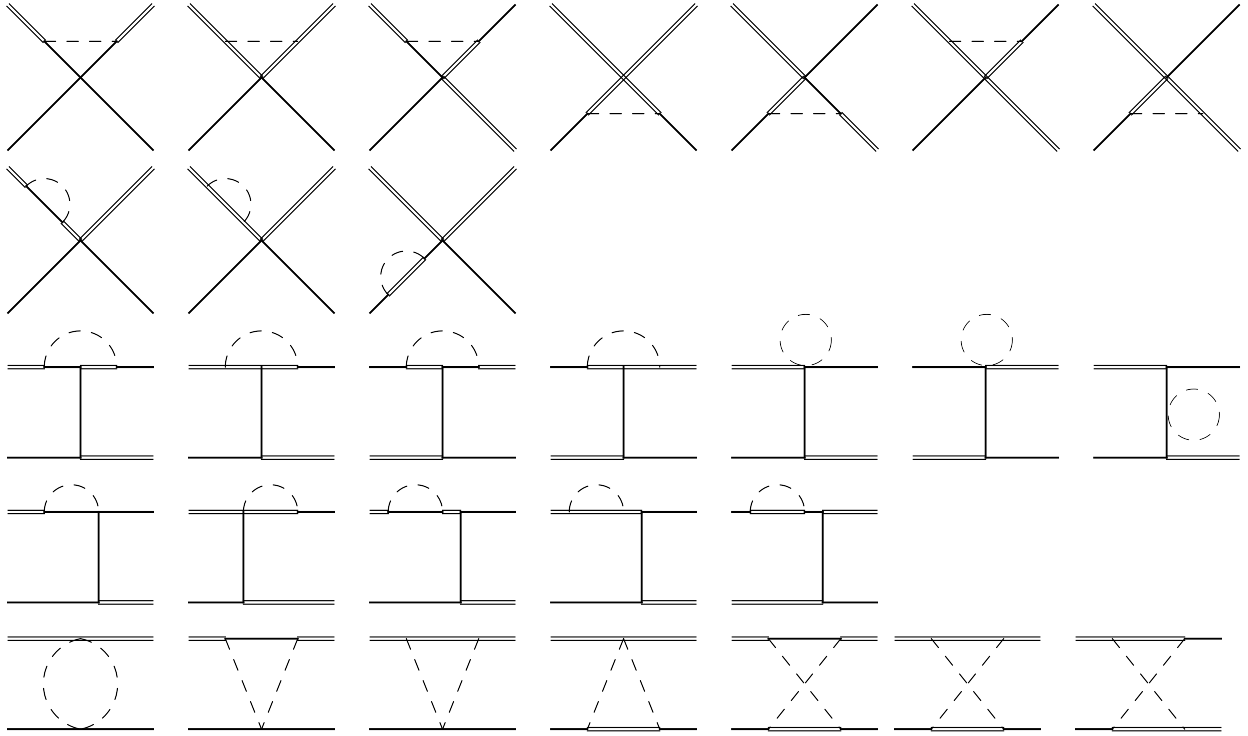


FIG. 2. One-loop 2PI diagrams of the DD^* system at $O(\epsilon^2)$. The solid, double-solid, and dashed lines stand for D , D^* , and π , respectively.

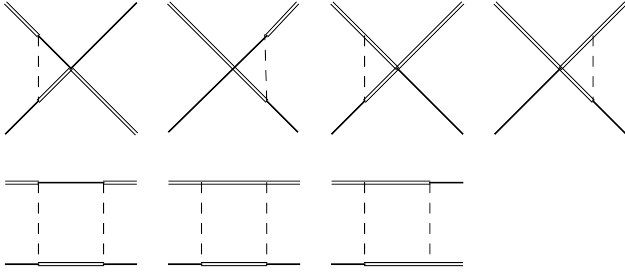


FIG. 3. One-loop 2PR diagrams of the DD^* system at $O(\epsilon^2)$. The solid, double-solid, and dashed lines stand for D , D^* , and π , respectively.

$$\begin{aligned}
& + 2\left[(d-3)q_0J_{11}^S(0)\vec{q}^2 - q_0J_{11}^T(-\delta)\vec{q}^2 + 3(d-3)q_0J_{22}^S(0)\vec{q}^2 - 3q_0J_{22}^T(-\delta)\vec{q}^2 + 2(d-3)J_{24}^S(0)\vec{q}^2 - 2J_{24}^T(-\delta)\vec{q}^2 \right. \\
& + 2(d-3)q_0J_{32}^S(0)\vec{q}^2 - 2q_0J_{32}^T(-\delta)\vec{q}^2 + 2(d-3)J_{33}^S(0)\vec{q}^2 - 2J_{33}^T(-\delta)\vec{q}^2 - (d-3)(d-2)q_0J_{21}^S(0) - q_0J_{21}^S(\delta) \\
& + (d-1)q_0J_{21}^T(-\delta) - 2(d-3)(d-2)q_0J_{31}^S(0) - 2q_0J_{31}^S(\delta) + 2(d-1)q_0J_{31}^T(-\delta) - 2(d-3)(d-2)J_{34}^S(0) - 2J_{34}^S(\delta) \\
& \left. + 2(d-1)J_{34}^T(-\delta)\right]g^2 + q_0^2J_0^F + 4q_0^2J_{11}^F + 4q_0^2J_{21}^F + 4J_{22}^F\left\{\epsilon \cdot \epsilon^* + \frac{2g^2}{16f^4}\left\{\frac{3}{2}\left[-3(d-3)J_{22}^B(\delta,0)\vec{q}^2 + 3J_{22}^B(-\delta,\delta)\vec{q}^2 \right. \right. \right. \\
& + (d-3)J_{22}^R(-\delta,0)\vec{q}^2 - J_{22}^R(-\delta,\delta)\vec{q}^2 - 6(d-3)J_{32}^B(-\delta,0)\vec{q}^2 + 6J_{32}^B(-\delta,\delta)\vec{q}^2 + 2(d-3)J_{32}^R(-\delta,0)\vec{q}^2 \\
& - 2J_{32}^R(-\delta,\delta)\vec{q}^2 - 3(d-3)J_{43}^B(-\delta,0)\vec{q}^2 + 3J_{43}^B(-\delta,\delta)\vec{q}^2 + (d-3)J_{43}^R(-\delta,0)\vec{q}^2 - J_{43}^R(-\delta,\delta)\vec{q}^2 + 6(d-3)J_{21}^B(-\delta,0) \\
& - 3J_{21}^B(-\delta,\delta) - (d-3)J_{21}^R(-\delta,0) + (d-3)J_{21}^R(-\delta,-\delta) + J_{21}^R(-\delta,\delta) + 3(d^2-9)J_{31}^B(-\delta,0) - 3(d+3)J_{31}^B(-\delta,\delta) \\
& - (d^2-9)J_{31}^R(-\delta,0) + (d+3)J_{31}^R(-\delta,\delta) + 3(d^2-9)J_{42}^B(-\delta,0) - 3(d+3)J_{42}^B(-\delta,\delta) - (d^2-9)J_{42}^R(-\delta,0) \\
& \left. \left. \left. + (d+3)J_{42}^R(-\delta,\delta)\right\}g^2 + 3(d-3)q_0J_{11}^S(0) - 3q_0J_{11}^S(\delta) + 9(d-3)q_0J_{22}^S(0) - 9q_0J_{22}^S(\delta) + 6(d-3)J_{24}^S(0) - 6J_{24}^S(\delta) \right\}
\end{aligned}$$

$$\begin{aligned}
& + 6(d-3)q_0J_{32}^S(0) - 6q_0J_{32}^S(\delta) + 6(d-3)J_{33}^S(0) - 6J_{33}^S(\delta) \Big\} q \cdot \varepsilon q \cdot \varepsilon^*, \\
\mathcal{V}_{2\pi(2)}^{l=1} = & \frac{-1}{16f^4} \Big\{ [(d-3)J_{22}^B(-\delta, 0)\vec{q}^4 + 5(d-3)J_{22}^R(-\delta, 0)\vec{q}^4 + 2(d-3)J_{32}^B(-\delta, 0)\vec{q}^4 + 10(d-3)J_{32}^R(-\delta, 0)\vec{q}^4 \\
& + (d-3)J_{43}^B(-\delta, 0)\vec{q}^4 + 5(d-3)J_{43}^R(-\delta, 0)\vec{q}^4 - 5(d-3)J_{21}^R(-\delta, 0)\vec{q}^2 - 5(d-3)J_{21}^R(-\delta, -\delta)\vec{q}^2 \\
& + ((5-2d)d+3)J_{31}^B(-\delta, 0)\vec{q}^2 - J_{31}^B(-\delta, \delta)\vec{q}^2 - 5(d-3)(2d+1)J_{31}^R(-\delta, 0)\vec{q}^2 - 5J_{31}^R(-\delta, \delta)\vec{q}^2 \\
& + ((5-2d)d+3)J_{42}^B(-\delta, 0)\vec{q}^2 - J_{42}^B(-\delta, \delta)\vec{q}^2 - 5(d-3)(2d+1)J_{42}^R(-\delta, 0)\vec{q}^2 - 5J_{42}^R(-\delta, \delta)\vec{q}^2 \\
& + (d-3)(d-2)(d+1)J_{41}^B(-\delta, 0) + (d+1)J_{41}^B(-\delta, \delta) + 5(d-3)(d-2)(d+1)J_{41}^R(-\delta, 0) + 5(d+1)J_{41}^R(-\delta, \delta) \Big] g^4 \\
& + 2 \Big[(d-3)q_0J_{11}^S(0)\vec{q}^2 - q_0J_{11}^T(-\delta)\vec{q}^2 + 3(d-3)q_0J_{22}^S(0)\vec{q}^2 - 3q_0J_{22}^T(-\delta)\vec{q}^2 + 2(d-3)J_{24}^S(0)\vec{q}^2 - 2J_{24}^T(-\delta)\vec{q}^2 \\
& + 2(d-3)q_0J_{32}^S(0)\vec{q}^2 - 2q_0J_{32}^T(-\delta)\vec{q}^2 + 2(d-3)J_{33}^S(0)\vec{q}^2 - 2J_{33}^T(-\delta)\vec{q}^2 - (d-3)(d-2)q_0J_{21}^S(0) - q_0J_{21}^S(\delta) \\
& + (d-1)q_0J_{21}^T(-\delta) - 2(d-3)(d-2)q_0J_{31}^S(0) - 2q_0J_{31}^S(\delta) + 2(d-1)q_0J_{31}^T(-\delta) - 2(d-3)(d-2)J_{34}^S(0) - 2J_{34}^S(\delta) \\
& + 2(d-1)J_{34}^T(-\delta) \Big] g^2 + q_0^2J_0^F + 4q_0^2J_{11}^F + 4q_0^2J_{21}^F + 4J_{22}^F \Big\} \varepsilon \cdot \varepsilon^* + \frac{-2g^2}{16f^4} \Big\{ \frac{1}{2} \Big[(d-3)J_{22}^B(-\delta, 0)\vec{q}^2 - J_{22}^B(-\delta, \delta)\vec{q}^2 \\
& + 5(d-3)J_{22}^R(-\delta, 0)\vec{q}^2 - 5J_{22}^R(-\delta, \delta)\vec{q}^2 + 2(d-3)J_{32}^B(-\delta, 0)\vec{q}^2 - 2J_{32}^B(-\delta, \delta)\vec{q}^2 + 10(d-3)J_{32}^R(-\delta, 0)\vec{q}^2 \\
& - 10J_{32}^R(-\delta, \delta)\vec{q}^2 + (d-3)J_{43}^B(-\delta, 0)\vec{q}^2 - J_{43}^B(-\delta, \delta)\vec{q}^2 + 5(d-3)J_{43}^R(-\delta, 0)\vec{q}^2 - 5J_{43}^R(-\delta, \delta)\vec{q}^2 + J_{21}^B(-\delta, \delta) \\
& - 5(d-3)J_{21}^R(-\delta, 0) - 5(d-3)J_{21}^R(-\delta, -\delta) + 5J_{21}^R(-\delta, \delta) - (d^2-9)J_{31}^B(-\delta, 0) + (d+3)J_{31}^B(-\delta, \delta) \\
& - 5(d^2-9)J_{31}^R(-\delta, 0) + 5(d+3)J_{31}^R(-\delta, \delta) - (d^2-9)J_{42}^B(-\delta, 0) + (d+3)J_{42}^B(-\delta, \delta) - 5(d^2-9)J_{42}^R(-\delta, 0) \\
& + 5(d+3)J_{42}^R(-\delta, \delta) \Big] g^2 + (d-3)q_0J_{11}^S(0) - q_0J_{11}^S(\delta) + 3(d-3)q_0J_{22}^S(0) - 3q_0J_{22}^S(\delta) + 2(d-3)J_{24}^S(0) - 2J_{24}^S(\delta) \\
& + 2(d-3)q_0J_{32}^S(0) - 2q_0J_{32}^S(\delta) + 2(d-3)J_{33}^S(0) - 2J_{33}^S(\delta) \Big\} q \cdot \varepsilon q \cdot \varepsilon^*, \tag{15}
\end{aligned}$$

where $C_1 = D_a + D_b - 3(E_a + E_b)$, $C_2 = D_a - D_b + E_a - E_b$, $C_3 = D_a + E_a$, $C_4 = D_b + E_b$, $C_5 = D_b - 3E_b$. In the above, d is the space-time dimension originated from the dimensional regularization, δ is the $D - D^*$ mass splitting, \mathcal{V} relates to the scattering amplitude \mathcal{M} via $\mathcal{V} = \mathcal{M}/(-\sqrt{\prod 2M_i} \prod 2M_f)$. The loop function J is defined in Refs. [33, 34]. In addition, considering the S -wave interactions we have $\vec{\varepsilon} \cdot \vec{\varepsilon}^* \mapsto 1$ and $\vec{\varepsilon} \cdot \vec{p} \vec{\varepsilon}^* \cdot \vec{p} \mapsto \vec{p}^2/(d-1)$.

Under Fourier transformation we can get the potential $\mathcal{V}(\mathbf{r})$:

$$\mathcal{V}(\mathbf{r}) = \int \frac{d\mathbf{p}}{(2\pi)^3} \mathcal{V}(\mathbf{p}) e^{i\mathbf{p}\cdot\mathbf{r}}, \tag{16}$$

where $\mathcal{V}(\mathbf{p})$ is a polynomial of \mathbf{p} , so the integral will be highly divergent with the increasing of the order.

C. The Subtraction of the 2PR contributions and the regularization of the potentials

To obtain a 2PI effective potential and further substitute it into the equations, we have to subtract the 2PR contributions appearing in all the 2PR diagrams, because they violate the power-counting rule and cause pinch singularities in our heavy hadron formalism.

Now take a closer look at a 2PR diagram, e.g. the box diagram (TPE contribution) in Fig. 2. When closing the energy contour integral, we are able to collect two poles in the loop function: the pion pole and the heavy meson pole. The pion

pole belongs to the 2PI part and satisfies the power-counting, whereas the heavy meson pole belongs to the iterated OPE contribution (i.e. 2PR part) and has an enhanced chiral order which violates the power-counting. Furthermore, the heavy meson poles located in upper and lower planes come too close, which produces a pinch singularity in the heavy hadron formalism. Therefore we have to preserve only the pion pole.

To collect the pion pole, in our previous work [34] we apply the substitution

$$\begin{aligned}
& \int d^4l \frac{1}{v \cdot l + a + i\varepsilon} \frac{1}{-v \cdot l - a + i\varepsilon} \times \dots \\
& \rightarrow \int d^4l \frac{1}{v \cdot l + a + i\varepsilon} (-1) \frac{1}{v \cdot l + a + i\varepsilon} \times \dots \tag{17}
\end{aligned}$$

when calculating the loop functions. However, such substitution only subtracts the heavy meson pole in the single channel diagrams (e.g. $DD^* \rightarrow D^*D \rightarrow DD^*$), the coupled-channel diagrams (e.g. $DD^* \rightarrow D^*D^* \rightarrow DD^*$) are intact. So we extend the subtraction to contain all the types of the 2PR diagrams:

$$\begin{aligned}
& \int d^4l \frac{1}{v \cdot l + a + i\varepsilon} \frac{1}{-v \cdot l - b + i\varepsilon} \times \dots \\
& \rightarrow \int d^4l \frac{1}{v \cdot l + a + i\varepsilon} (-1) \frac{1}{v \cdot l + b + i\varepsilon} \times \dots \tag{18}
\end{aligned}$$

Note that although the 2PR parts of the coupled-channel 2PR diagrams avoid the pinch singularities due to a tiny separation of the two heavy meson poles (originated from the mass

splitting δ), their contributions are still abnormally enhanced ($\sim 1/\delta$). Therefore the subtractions of these contributions are surely needed.

After discussing the subtraction of the 2PR contributions, we now turn to the regularization of the calculated 2PI potential. In previous work [1, 34], we use a simple Gaussian cutoff $\exp(-\vec{q}^{2n}/\Lambda^{2n})$ to regularize the potential. However, simple use of this regulator leads to two drawbacks in the TPE calculation: an overestimation of the TPE as well as a highly sensitive dependence on the cutoff Λ .

The reason is that, the calculated TPE potential is a polynomial of momentum \vec{q} (especially contains the terms of high \vec{q} power), this NLO contribution just shows a good convergence within a low \vec{q} region (empirically say, up to 2π mass, around 300 MeV). When we apply $\exp(-\vec{q}^{2n}/\Lambda^{2n})$, the main contribution of the potential will come from the region $|\vec{q}| \lesssim \Lambda$. So if Λ is below 300 MeV, the convergence would be quite good, i.e. the TPE contribution (NLO) would be relatively small. But in practice, Λ is generally chosen to be 500 ~ 1000 MeV, it mean that the contributions in the region $|\vec{q}| \lesssim 500$ (~ 1000) MeV are all included, which breaks up the convergence and causes TPE abnormally large. Actually, with the increase of Λ , the contributions from high \vec{q} region will grow rapidly and become dominant, note that these contributions mainly attribute to the terms of high \vec{q} powers in the potential.

As we discussed above, with a relatively high Λ , the main contribution of the potential comes from high \vec{q} region and the terms of high \vec{q} powers, it means the TPE is dominated by short distance contribution. In the coordinate space, It would result in a short distance potential which is singular even than the contact contribution. Therefore, if insist to use the practically determined Λ , we need to suppress the contribution of the TPE in the region $m_{\text{ch}} \lesssim |\vec{q}| \lesssim \Lambda$ (where m_{ch} is typically around 2π mass, about 300 MeV) in addition to the regulator $\exp(-\vec{q}^{2n}/\Lambda^{2n})$.

So in this work, we propose three different schemes to deal with the above problems in TPE potential:

scheme I: As we explained above, the chiral expansion is reasonable, while the high \vec{q} contribution is excluded, only when cutoff Λ is low, so we just constrain Λ to 0 ~ 450 MeV here. in this case we do not need to introduce additional strategies to suppress the TPE. However, due to the low chosen Λ , the potential may become less attractive with the already fixed LECs, therefore in this scheme we refit the LECs.

scheme II: In this scheme we do not constrain the Λ , instead we introduce an regulator $\mathcal{F}_{2\pi}(\vec{q})$ to the TPE contribution in addition to the overall regulator $\exp(-\vec{q}^{2n}/\Lambda^{2n})$. The purpose of $\mathcal{F}_{2\pi}(\vec{q})$ is to constrain the highly divergent contribution beyond $|\vec{q}| = m_{\text{ch}}$. For $\mathcal{F}_{2\pi}(\vec{q})$ we use

$$\mathcal{F}_{2\pi}(\vec{q}) = \left(\frac{\mu_{2\pi}^2}{\vec{q}^2 + \mu_{2\pi}^2} \right)^{n_{2\pi}} \quad (19)$$

with $n_{2\pi} = 4$. We adjust $\mu_{2\pi}$ so that the strength of the TPE outside perturbation region ($|\vec{q}| \gtrsim m_{\text{ch}}$) does not surpass the strength in $|\vec{q}| \lesssim m_{\text{ch}}$.

scheme III: In this scheme we also do not constrain the Λ , however different from *scheme II* we adopt another strategy to

suppress the TPE. We preserve the contribution in the region $|\vec{q}| \lesssim m_{\text{ch}}$, then, we set the momentum potential $\mathcal{V}_{2\pi}^{\text{III}}(\vec{q})$ (superscript III stands for scheme III) to a constant starting from $|\vec{q}| = m_{\text{ch}}$, i.e.,

$$\mathcal{V}_{2\pi}^{\text{III}}(\vec{q}) = \begin{cases} \mathcal{V}_{2\pi}(\vec{q}) & |\vec{q}| \leq m_{\text{ch}}, \\ \mathcal{V}_{2\pi}(m_{\text{ch}}) & |\vec{q}| \geq m_{\text{ch}}, \end{cases} \quad (20)$$

where $\mathcal{V}_{2\pi}(\vec{q})$ is the unmodified TPE contribution. As we discussed above, we choose $m_{\text{ch}} = 300$ MeV. This scheme has advantages over the scheme II: it not only suppresses the TPE in the high \vec{q} region, but lets the TPE having the same ultraviolet behavior as the OPE and contact (they are both constants in the large $|\vec{q}|$ region), as we will discuss below.

Here we give some comments on the schemes II and III. When we look into the individual contributions of contact, OPE and TPE in momentum space later in Fig. 4, we can find that with the increase of \vec{q} , the contact and OPE tend to constants because of the contact terms in them, which means that their sensitivities on Λ are same. It further indicates that the two contributions can adopt a same regularization procedure, i.e. they may be regularized with a same regulator as well as same Λ . However the TPE is not the case. The TPE contribution goes to infinity because of the terms of high \vec{q} power, so its ultraviolet behavior is different from that of the contact or OPE. Consequently the TPE is very sensitive on the cutoff parameter Λ , so a different regularization or Λ may be applied. This is the reason we introduce the scheme II and scheme III.

Especially in scheme III, we set the TPE to a constant beyond m_{ch} within which the expansion is valid, so that all three contributions have consistent ultraviolet behaviors, based on this we are ready to apply an unified regularization scheme to them.

At last, note that in all the schemes including I, II and III, we all apply the following overall regulator $\mathcal{F}(\vec{q})$ to the contact, OPE and TPE contributions:

$$\mathcal{F}(\vec{q}) = \exp(-\vec{q}^{2n}/\Lambda^{2n}). \quad (21)$$

Of course we emphasize again that, besides $\mathcal{F}(\vec{q})$ the TPE are further dealt with using Eq. (19) (scheme II) or Eq. (20) (scheme III).

III. NUMERICAL RESULTS OF THE DD^* POTENTIALS

With the calculated expressions of $\mathcal{V}(q)$, the 2PR subtraction scheme as well as the proposed regularization schemes in Sec. II C, we now present the numerical results and discuss the behaviors of the DD^* potentials with different schemes in detail. In this work we use the input parameters following Refs [1, 34], especially the low energy constants $D_a^{\text{RSM}} = -6.62$, $E_a^{\text{RSM}} = -5.74$, $D_b^{\text{RSM}} = 0$ and $E_b^{\text{RSM}} = 0$, where RSM means they are obtained using the resonance saturation model. In addition, we use $q^0 = \delta$.

A. The original DD^* potentials in momentum space

In this subsection we discuss the potentials in momentum space without any scheme applied, i.e. with only overall regulator $\mathcal{F}(\vec{q})$ (21) attached. We list the results in Fig. 4. Here we consider the $I = 0$ channel. Note that $q = |\vec{q}|$ is the 3-momentum in the Fig 4.

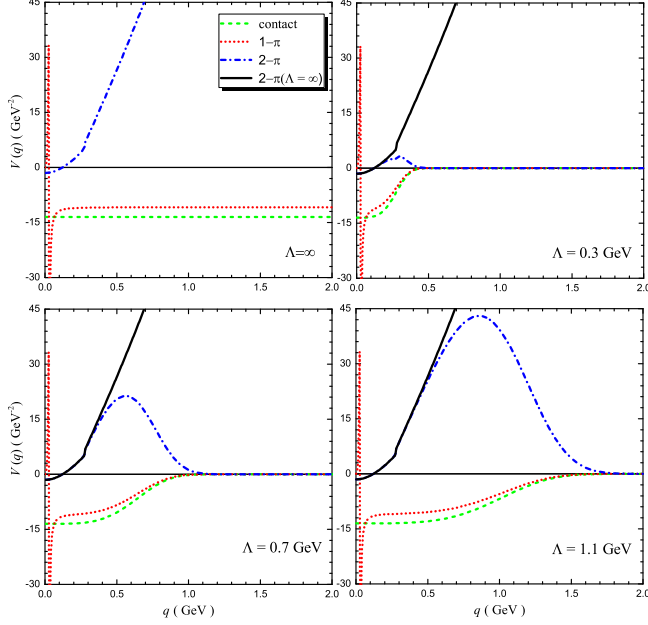


FIG. 4. The original $I = 0$ DD^* potentials $\mathcal{V}(q)$ in momentum space attached with only overall regulator (21), varying with cutoff Λ . Note that $\Lambda = \infty$ just stands for the totally unregularized case. $q = |\vec{q}|$ is the 3-momentum in units of GeV.

From Fig. 4 we can see that, for the results without the regulator ($\Lambda = \infty$), when we restrict ourselves to the low q region (e.g. $q \leq 0.3$ GeV) the $O(\epsilon^2)$ TPE is small, which means that the convergence of our chiral expansion series is good. Move sights to the high q region, the contact and OPE contributions both tend to finite constants with the increase of q , which is reasonable because they have zeroth power of q . But the TPE contribution rapidly goes to divergence with the increase of q because of the terms of high q power in TPE, so its convergence surely breaks up. As we discussed before, it may indicate that the contact and OPE can be applied with a same regularization scheme while the TPE can not be. In conclusion, the high q behavior of the TPE is totally different from that of the contact or OPE. So we indeed need to adopt a distinctive regularization strategy for the TPE contribution.

We now focus on the results with the overall regulator $\mathcal{F}(\vec{q})$ turning on. At $\Lambda = 0.3$ GeV, when looking at the general line shape we observe that the TPE contribution is small comparing to the contact and OPE contributions, which shows a good convergence. As we explained in previous section, a low Λ means only the contribution within the low q region is preserved. When moving the cutoff to a higher value ($\Lambda = 0.7, 1.1$ GeV) in Fig. 4, we see the suppressed higher region con-

tributions are gradually recovered. Among them, the TPE is much more sensitive to the Λ than the contact and OPE, and it consequently becomes abnormally large at a high Λ , so that its relative magnitude is far beyond the contact and OPE contributions. As we dictated in the previous section, such TPE will become a short-distance interaction which is singular even than the contact. In a word, the TPE should be treated differently in the regularization procedure.

We also mention that in Fig. 4, the regularized TPE preserves the unregularized TPE potential (black line) in the low q region, while in the high q region they are suppressed to zero by $\mathcal{F}(\vec{q})$. So the use of the regulator (21) is reasonable because the low momentum contributions are well preserved.

At last, we discuss the general behaviors of all the contributions. From Fig. 4 we see the contact and OPE are attractive while the TPE is repulsive. The judgment of the repulsive TPE is one of our most important conclusions. Note that, it is consistent with the results of the $I = 0$ $\bar{B}\bar{B}^*$ system where $\delta = 0$ limit is considered [36], and also consistent with the $D^{(*)}\bar{B}^{(*)}$ calculation in Ref. [35].

B. DD^* potentials in scheme I

Through the above investigations we speculate that a careful treatment of the TPE is needed. So in this subsection we show the results applying scheme I. In this scheme other than using an additional regularization on the TPE, we actually restrict cutoff Λ to a low value to maintain the convergence as well as suppress the high q contribution.

We first show the $I = 0$ results in momentum space in Fig. 5. Here we choose three typical Λ values: 0.25 GeV, 0.35 GeV and 0.45 GeV. We can find that at these Λ , the TPE are indeed not very large, so in these cases the expansions show good convergences. As we discussed in Sec. II C this is because the chosen Λ can cutoff the contribution beyond $q = \Lambda$, so the high q contribution in TPE is just suppressed by such low Λ .

Next we show the $I = 0$ potentials in coordinate space in Fig. 6. We find that, the TPE contributions in the potentials $\mathcal{V}(r)$ are still not very large, which is consistent with the observation about the momentum potentials $\mathcal{V}(q)$. So if we do not want to additionally tackle with the TPE, we choose the strategy that restricts the Λ to a low value. Also, we can observe an important feature in this scheme: because of the adopted low Λ , the potentials span across large distances and generally reach beyond 10 GeV $^{-1}$ (2 fm), while the magnitudes of the potentials are relatively small. Especially for $\Lambda = 0.25$ GeV, the potential can arrive at 20 GeV $^{-1}$ (4 fm). It means that at these low Λ , they are very long range potentials.

By solving the Schrödinger equation with the $I = 0$ $\mathcal{V}(r)$ at $\Lambda = 0.45$ GeV, we fit the binding energy to the location of the observed T_{cc} state by justifying the LEC D_a and E_a . Note that for illustration, we do not search for the parameter region of the LECs, but vary them around previous D_a^{RSM} and E_a^{RSM} with a same multiplier: $D_a = cD_a^{\text{RSM}}$, $E_a = cE_a^{\text{RSM}}$. Here we get $c = 2.7$ at $\Lambda = 0.45$ GeV, and we show the potential $\mathcal{V}(r)$

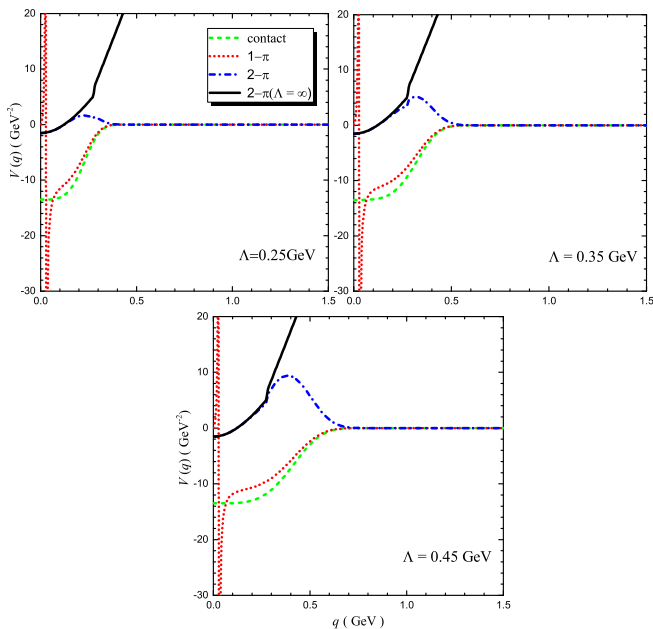


FIG. 5. The $I = 0 DD^*$ potentials $\mathcal{V}(q)$ under scheme I, varying with cutoff Λ . $q = |\vec{q}|$ is the 3-momentum in units of GeV.

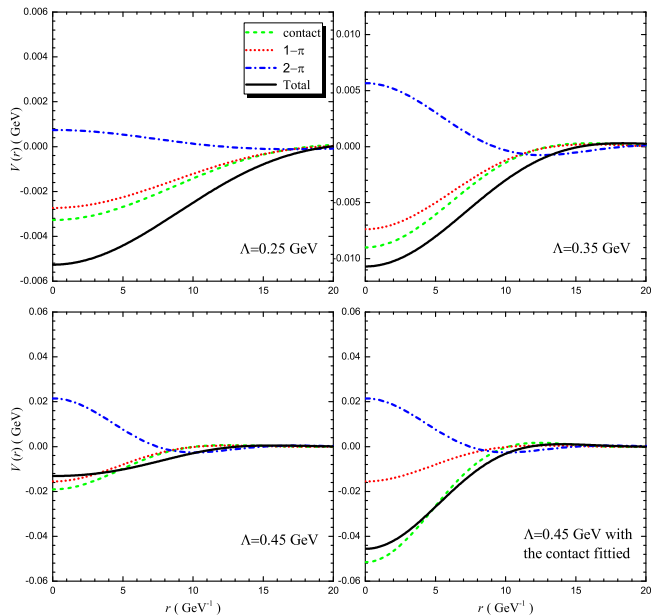


FIG. 6. The $I = 0 DD^*$ potentials $\mathcal{V}(r)$ under scheme I, varying with cutoff Λ . Note that the LECs of the contact contribution in the last diagram are fitted to T_{cc} mass.

with the fitted LECs in the last diagram of Fig. 6.

From this diagram we can see that, the competition between the powerful repulsing TPE and the other two (contact and OPE) leads to a quite weak attraction, this explains why T_{cc} has a extremely small binding energy if treated as the $I = 0 DD^*$ bound state. Therefore we believe the repulsive nature

of the TPE in our framework accords with the experimental observation. On the other hand, if the TPE is attractive, we expect all three attractive contributions should have caused a much deeper $I = 0 DD^*$ bound state.

The above feature of T_{cc} ($I = 0 DD^*$) is also very similar to that of $X(3872)$ ($I = 0 DD^*$) presented in our previous work [1]. In Ref. [1], we find that for $X(3872)$ treated as a $0^+ 1^{++} DD^*$ bound state, its TPE is repulsive while the contact and OPE are attractive, which leads to a small binding energy. In a word, this common feature shared by $X(3872)$ and T_{cc} , especially the repulsive TPE, is much responsible for their extremely near-threshold phenomena.

C. DD^* potentials in scheme II

Here we will apply scheme II to deal with the TPE contribution. As we discussed before, in this scheme we apply an additional factor $\mathcal{F}_{2\pi}(\vec{q})$ (19) to constrain the TPE outside the perturbation region ($|\vec{q}| \gtrsim m_{ch}$). Assuming $\mathcal{V}_{2\pi}(\vec{q})$ is the unmodified TPE contribution and $\mathcal{V}_{2\pi}^{II}(\vec{q}) = \mathcal{V}_{2\pi}(\vec{q})\mathcal{F}_{2\pi}(\vec{q})$ where superscript ‘‘II’’ stands for scheme II, we let $\mathcal{V}_{2\pi}^{II}(\vec{q}) \leq \mathcal{V}_{2\pi}(m_{ch})$ in the region $|\vec{q}| \gtrsim m_{ch}$, and obtain the adjusted parameter $\mu_{2\pi} = 1.0$ GeV.

Then we show the $I = 0$ potential in momentum space in Fig. 7. At $\Lambda = \infty$ (without $\mathcal{F}(\vec{q})$), we see the TPE contribution in high q region (blue-dash-dot line) is now largely suppressed comparing to the highly divergent unmodified TPE (black-solid line). In this case, the maximum amount of the TPE is limited just as the contact and OPE (because they both are almost constants at high q). Consequently, we can see that when Λ varies from 0.3 GeV to 1.1 GeV, all three contributions possess a same behavior with the increase of Λ : the sensitivities on Λ are almost same. So the TPE is no longer dominant over other two at high Λ . In other words, it solves the problem discussed in Sec. II C.

In Fig. 8 we show the $I = 0$ potentials $\mathcal{V}(r)$ in coordinate space. As we expect the behavior of the TPE contribution is consistent with the $\mathcal{V}(q)$ showing in Fig. 7: the TPE grows smoothly when Λ varying from 0.3 GeV to 1.1 GeV, also it does not get enormously large at high Λ . Comparing to scheme I, the ranges they stretch to are generally shorter, because in this scheme the adopted Λ varies up to 1.1 GeV. As we have discussed in Sec. II C, when a high Λ is applied, the contributions in the high q region $m_{ch} \lesssim q \lesssim \Lambda$ are all counted in, these contributions will make the potential tend to a short distance.

In this scheme, when Λ varies to 0.95 GeV, the T_{cc} state is produced. The corresponding potentials $\mathcal{V}(r)$ are also depicted in Fig. 8. In Fig. 8, as we discussed in scheme I the competition between TPE and the other two leads to the observed near-threshold phenomenon of T_{cc} .

D. DD^* potentials in scheme III

We now show the results in scheme III. As we said in this scheme we constrain the TPE using Eq. (20). This scheme

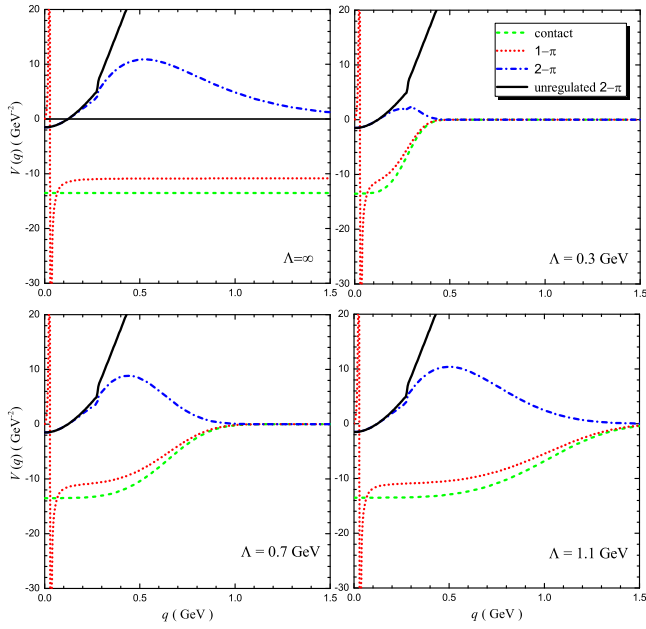


FIG. 7. The $I = 0$ DD^* potentials $\mathcal{V}(q)$ under scheme II, varying with cutoff Λ . $q = |\vec{q}|$ is the 3-momentum in units of GeV. The “unregulated $2\text{-}\pi$ ” stands for the totally unmodified TPE contribution ($\Lambda = \infty, \mu_{2\pi} = \infty$).

has an advantage over scheme II : the TPE and other two contributions will have a same high momentum behavior, so that we can confidently use the same regularization scheme (21) on them.

We depict the potentials in momentum space varying with Λ in Fig. 9. From the $\Lambda = \infty$ case we see, in this scheme the TPE goes to a constant just as other contributions. As we discussed in Sec. II C, in this situation all contributions have a same high q (ultraviolet) behavior, so we are able to use the same regularization procedure (Eq. (21)) on them. It brings a profitable consequence that all three contributions have highly consistent dependences on the Λ , as we show in Fig. 9 with Λ varying from 0.3 GeV to 1.1 GeV.

In Fig. 10 we present the potentials $\mathcal{V}(r)$. The variations of $\mathcal{V}(r)$ on Λ are consistent with $\mathcal{V}(q)$ in Fig. 9, especially the TPE here also rises synchronously with the contact and OPE. At $\Lambda = 0.94$ GeV, the potential $\mathcal{V}(r)$ can produce the T_{cc} state when substituted in the Schrödinger equation. So we can see the near-threshold nature of the T_{cc} state originates from the competition between the TPE and the other two, which has been already emphasized in scheme I and II.

As we can see, both scheme III and II preserve the TPE contribution in the low q region while modify that in the high q region, so that the high q behavior of the TPE is unified with that of the contact and OPE, which enables us to apply the common regularization (21) and further leads to similar Λ dependences for the three. However, comparing Fig. 7 and 9, we can find scheme II completely cutoffs the high q contribution whereas scheme III retains it to let the TPE coincide with the contact and OPE at high q . Due to the identical high q

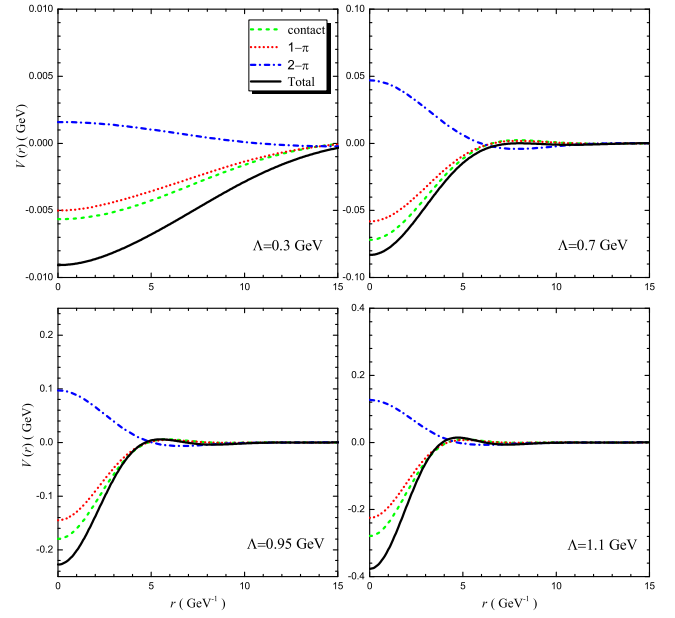


FIG. 8. The $I = 0$ DD^* potentials $\mathcal{V}(r)$ under scheme II, varying with cutoff Λ . Note that the potentials at $\Lambda = 0.95$ GeV correspond to the observed T_{cc} .

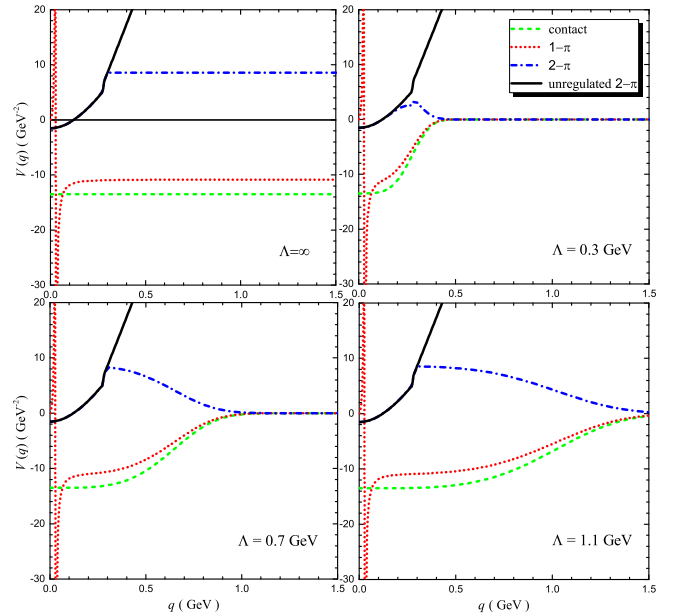


FIG. 9. The $I = 0$ DD^* potentials $\mathcal{V}(q)$ under scheme III, varying with cutoff Λ . $q = |\vec{q}|$ is the 3-momentum in units of GeV. The “unregulated $2\text{-}\pi$ ” stands for the totally unmodified TPE contribution ($\Lambda = \infty$, and no application of Eq. (20)).

behaviors of the contact, OPE and TPE, then the identical Λ dependences of the three, obviously scheme III is better.

Note that although the TPE of the two schemes in high q region have totally different behaviors, both they are largely cut by the regulator (21), so their final potentials $\mathcal{V}(r)$ in Fig. 8

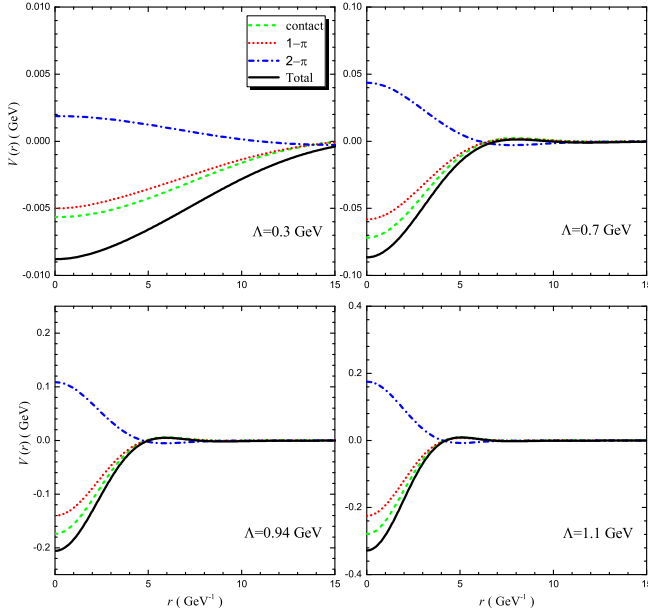


FIG. 10. The $I = 0$ DD^* potentials $\mathcal{V}(r)$ under scheme III, varying with cutoff Λ . Note that the potentials at $\Lambda = 0.94$ GeV correspond to the observed T_{cc} .

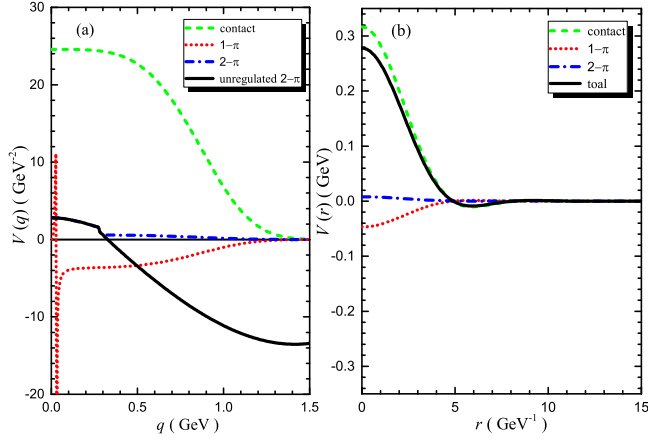


FIG. 11. The $I = 1$ DD^* potentials under scheme III: (a) the potentials $\mathcal{V}(q)$; (b) the potentials $\mathcal{V}(r)$. $q = |\vec{q}|$ is the 3-momentum in units of GeV. The “unregulated 2- π ” stands for the totally unmodified TPE contribution ($\Lambda = \infty$, and no application of Eq. (20)).

and 10 present not much discrepancies.

E. $I = 1$ DD^* potentials

Having discuss the $I = 0$ DD^* potentials in the different schemes, we now show the $I = 1$ potentials. Here we adopt scheme III.

We first depict the $I = 1$ DD^* potentials in momentum space in Fig. 11(a). We can find that the contact contribution

is dominant over the small OPE and TPE, it is also repulsive.

The $I = 1$ DD^* potentials in coordinate space are shown in Fig. 11(b). Consistent with the $\mathcal{V}(q)$ in Fig. 11(a), the contact potential is dominant and repulsive. So the total potential $\mathcal{V}(r)$ behaves as a strong repulsive force. Indeed, when solving the Schrödinger equation we can not find a bound state solution within a wide range of Λ .

IV. SOLVING THE BS EQUATION WITH THE DD^* CHIRAL INTERACTIONS

In this section we alternatively solve the BS equation to see the consistency between the results of the two equations.

A. The DD^* BS equation and interaction kernels

In this subsection we first reduce the BS equation, then give the expressions of the DD^* interaction kernels.

For the DD^* system carrying momentum K and mass M , after the center of mass motion is removed the BS wave function is defined as

$$\begin{aligned} \chi_{ij}^{I\mu}(x, K) &= \langle 0 | T [\mathcal{D}_i(\lambda_2 x) \mathcal{D}_j^{*\mu}(-\lambda_1 x)] | I; K \rangle \\ &= C_{I, I_3}^{ij} \chi^{I\mu}(x, K). \end{aligned} \quad (22)$$

Here $\mathcal{D}(\mathcal{D}^{*\mu})$ is the field operator of $D(D^*)$ meson, x is the relative coordinate between D and D^* , and we assume $D(D^*)$ possesses the momentum $k_1(k_2)$ and mass $m_1(m_2)$. The subscript $i(j) = 1, 2$ is the flavor index, I and I_3 are isospin and third component respectively, also $\lambda_{1(2)} = m_{1(2)}/(m_1 + m_2)$. Note that in above the isospin coefficients C_{I, I_3}^{ij} are determined according to the isospin wave functions (5):

$$\begin{aligned} C_{0,0}^{12} &= \frac{1}{\sqrt{2}}, & C_{0,0}^{21} &= -\frac{1}{\sqrt{2}}, \\ C_{1,0}^{12} &= \frac{1}{\sqrt{2}}, & C_{1,0}^{21} &= \frac{1}{\sqrt{2}}, \\ C_{1,1}^{22} &= 1, & C_{1,-1}^{11} &= 1. \end{aligned} \quad (23)$$

The BS wave function in momentum space $\chi_{ij}^{I\mu}(k, K)$ is defined via

$$\chi_{ij}^{I\mu}(x, K) = \int \frac{d^4 k}{(2\pi)^4} \chi_{ij}^{I\mu}(k, K) e^{-ikx}, \quad (24)$$

where k is the relative momentum between D and D^* . Using k we also have $k_1 = \lambda_1 K + k$, $k_2 = \lambda_2 K - k$. $\chi_{ij}^{I\mu}(k, K)$ satisfies the following homogeneous integral equation:

$$\chi_{ij}^{I\mu}(k, K) = s_D(k_1) s_{D^*}^{*\mu}(k_2) \int \frac{d^4 l}{(2\pi)^4} \chi_{mn}^{I,\alpha}(l, K) \mathcal{K}_{mni, \alpha\nu}(l, k, K), \quad (25)$$

where $s_{D^{(*)}}$ is the propagator for $D^{(*)}$, \mathcal{K} is the interaction kernel. Notice that l is a relative momentum too, so that $l_1 =$

$\lambda_1 K + l$ and $l_2 = \lambda_2 K - l$. Taking into account $\chi_{ij}^{I,\mu} = C_{I,l_3}^{ij} \chi^{I,\mu}$ and C_{I,l_3}^{ij} values (23), we reduce Eq. (25) to the equation of $\chi^{I,\mu}$:

$$\chi^\mu(k) = s_D(k_1) s_{D^*}^{\nu\mu}(k_2) \int \frac{d^4 l}{(2\pi)^4} \mathcal{K}_{\alpha\nu}^I(l, k, K) \chi^\alpha(l), \quad (26)$$

where χ^μ is the abbreviation of $\chi^{I,\mu}$. The specific $I = 0, 1$ kernels \mathcal{K} read:

$$\begin{aligned} \mathcal{K}_{\alpha\nu}^{I=0}(l, k, K) &= \mathcal{K}^{D^0 D^{*+} \rightarrow D^0 D^{*+}}(l, k, K) - \mathcal{K}^{D^+ D^0 \rightarrow D^0 D^{*+}}(l, k, K), \\ \mathcal{K}_{\alpha\nu}^{I=1}(l, k, K) &= \mathcal{K}^{D^0 D^{*+} \rightarrow D^0 D^{*+}}(l, k, K) + \mathcal{K}^{D^+ D^0 \rightarrow D^0 D^{*+}}(l, k, K). \end{aligned} \quad (27)$$

Note that in general a kernel is expressed as a function of the momentum transfer q and p : $\mathcal{K}(l, k, K) = \mathcal{K}(p, q, K)$ with relations $q = l_1 - k_1$ and $p = l_1 - k_2$.

For solving the equations later we decompose the relative momentum k into the longitudinal and transverse parts: $k = k_\ell v + k_t$, $v \cdot k_t = 0$, with $v = K/M$ being the four velocity of the DD^* system. Here we consider the instantaneous approximation: $\mathcal{K}(p, q, K) \simeq \mathcal{K}(p_t, q_t, K)$. In this approach we need to integrate out the longitudinal part of Eq. (26) to arrive at a three dimension integral equation. Defining $\chi^\mu(k_t) = \int dk_\ell / 2\pi \chi^\mu(k)$, we perform the contour integrals $\int dk_\ell / 2\pi$ on both sides of Eq. (26) and obtain

$$\begin{aligned} \chi^\mu(k_t) &= \int \frac{d^3 l_t}{(2\pi)^3} \left[\frac{-i(-g^{\nu\mu} + k_2^\nu k_2^\mu / m_2^2)}{(-2\omega_1)(M + \omega_1 + \omega_2)(M + \omega_1 - \omega_2)} \right]_{k_t = -(\lambda_1 M + \omega_1)} \\ &\quad + \frac{i(-g^{\nu\mu} + k_2^\nu k_2^\mu / m_2^2)}{(M - \omega_2 + \omega_1)(M - \omega_2 - \omega_1)(2\omega_2)} \Big|_{k_t = \lambda_2 M - \omega_2} \Big] \mathcal{K}_{\alpha\nu}^I(p_t, q_t, K) \\ &\quad \times \chi^\alpha(l_t), \end{aligned} \quad (28)$$

with $\omega_i = \sqrt{m_i^2 - k_t^2}$.

We consider the $J^P = 1^+$ state only, so the BS wave function $\chi^\mu(k_t)$ can be constructed as

$$\chi^\mu(k_t) = \varepsilon^\mu(K) \varphi(k_t). \quad (29)$$

In addition, we normalize the obtained BS wave function with

$$i \int \frac{d^4 k}{(2\pi)^4} \frac{d^4 l}{(2\pi)^4} \bar{\chi}^\mu(k) \left[\frac{\partial}{\partial K^0} I_{\mu\nu}(k, l, K) \right] \chi^\nu(l) = 2K^0. \quad (30)$$

According to the 2PI diagrams in Figs. 1 and 2, we now calculate $\mathcal{K}^{I=0,1}$ (defined in Eq. (27)) up to the order $O(\varepsilon^2)$. Here we show the \mathcal{K} at order $O(\varepsilon^0)$,

$$\mathcal{K}_{\text{contact}(0)}^{I=0,\mu\nu} = -8im_1 m_2 (D_a + D_b - 3E_a - 3E_b) g^{\mu\nu}, \quad (31)$$

$$\mathcal{K}_{\text{contact}(0)}^{I=1,\mu\nu} = -8im_1 m_2 (D_a - D_b + E_a - E_b) g^{\mu\nu}, \quad (32)$$

$$\mathcal{K}_{1\pi(0)}^{I=0,\mu\nu} = -3im_1 m_2 \frac{g^2}{f^2} \frac{1}{p^2 - m^2} p^\mu p^\nu, \quad (33)$$

$$\mathcal{K}_{1\pi(0)}^{I=1,\mu\nu} = -im_1 m_2 \frac{g^2}{f^2} \frac{1}{p^2 - m^2} p^\mu p^\nu, \quad (34)$$

while \mathcal{K} at order $O(\varepsilon^2)$ are collected in Appendix A.

B. The numerical results

Here we solve the obtained BS equation above numerically. For the regularization of the TPE we adopt scheme III (20). Note that due to the distinct formalism comparing to the Schrödinger equation, the application of scheme III here is slightly different. For the terms with the structure $g^{\mu\nu}$ in the kernels \mathcal{K} , we just apply Eq. (20), while for the terms with the structure $q^\mu q^\nu$ (or $p^\mu p^\nu$), we replace $q^\mu q^\nu$ with $q^\mu q^\nu m_{\text{ch}}^2 / \vec{q}^2$ beyond $|\vec{q}| = m_{\text{ch}}$ for consistency.

After solving the BS equation, we obtain bound state solutions at some typical Λ values, which are listed in Table I. We can see that the $I = 0$ channel has a bound state solution emerging at around $\Lambda = 0.79$ GeV, and the binding energy increases with the variation of Λ . Also, the solution at $\Lambda = 0.79$ corresponds to the observed T_{cc} state. While for the $I = 1$ channel there does not exist any solution in all Λ range. These conclusions are surely consistent with those obtained by solving the Schrödinger equation in Sec. III.

TABLE I. The bound state solutions of the DD^* BS equations in the $I = 0, 1$ channels. The cutoff parameter Λ , calculated mass M , and binding energy E relative to the $D^0 D^{*+}$ threshold are in units of GeV, MeV, and MeV, respectively. Note that the solution at $\Lambda = 0.79$ GeV corresponds to the observed T_{cc} state.

Λ	$I = 0$		$I = 1$	
	M	E	M	E
0.5	–	–	–	–
0.6	–	–	–	–
0.79	3874.7	0.36	–	–
0.8	3874.2	0.89	–	–
0.9	3869.9	5.19	–	–
1.0	3860.8	14.29	–	–
1.1	3845.8	29.29	–	–
1.3	3796.8	78.90	–	–
1.5	3705.8	169.29	–	–

Here we also depict the normalized scalar BS wave function $\varphi(k_t)$ of Eq. (29) in Fig. 12. From Fig. 12, we can find that the behavior of $\varphi(k_t)$ accords with that of the typical bound state wave function.

V. SUMMARY

In this work, we studied the DD^* interactions under chiral effective field theory (ChEFT). Within heavy hadron formalism, we calculate the DD^* potentials up to order $O(\varepsilon^2)$ (NLO) at 1-loop level. Comparing to our previous work [34], we adopt a new 2PR subtraction scheme for the 2PR digrams, and introduce multiple regularization strategies uniquely for the TPE contributions. We elaborately discuss the potential behaviors in the different regularizations of the TPE. At last we solve the Schrödinger equations with the obtained potentials, and search for the bound state solutions as well as their relations to the experimental findings. In addition, we also solve the BS equations of the DD^* interactions for a consistency check.

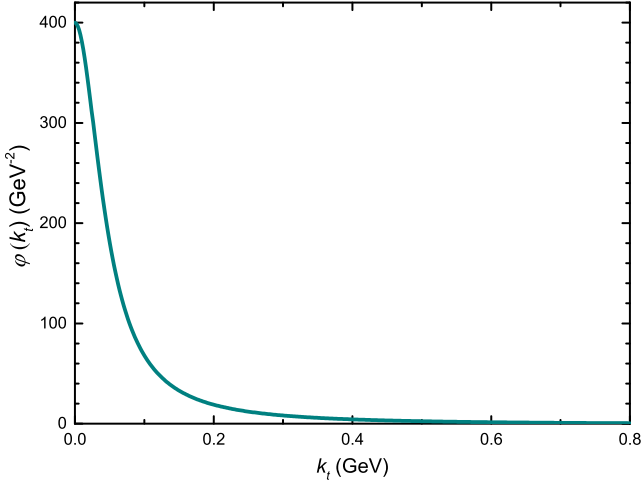


FIG. 12. The obtained $I = 0$ DD^* BS wave function $\varphi(k_i)$ which corresponds to the solution at $\Lambda = 0.79$ GeV, i.e. the T_{cc} state. k_i denotes the 3-momentum $|\vec{k}_i|$ in units of GeV.

Specifically, among the investigation, our improvements of the framework are as follows. First, due to the intermediate D^*D^* states as the coupled channel appearing in some 2PR diagrams, we apply a proper 2PR subtraction method to remove the additional poles brought by the coupled channels, so that all the heavy meson poles are just subtracted. Second, because the TPE contribution is highly divergent on the momentum transfer q far more than the contact and OPE, we believe a distinctive regularization may be imposed on the TPE. So in this work we propose three schemes to investigate the TPE regularization. Among them, one scheme applies a unified regulator for All three contributions, and other two adopt

unique regularizations for the TPE. All three schemes lead to similar conclusions, as we shall list below.

Here we list our main conclusions and key findings. We find that, there exists a bound state solution in the $I = 0$ channel, while no solution can be found in the $I = 1$ channel, so the observed T_{cc} state indeed can be treated as the $I = 0$ DD^* bound state. However, the interaction detail is most interesting: For the $I = 0$ T_{cc} state the TPE contribution is repulsive, then the competition between the repulsing TPE and other two contributions leads to a quite weak attraction. This just explains why the binding energy of T_{cc} is extremely small.

The above feature of T_{cc} just resembles $X(3872)$. As we indicated in Ref. [1], small binding energy of $X(3872)$ also comes from the balance between the repulsing TPE and the other two if it is treated as a $0^+1^{++} D\bar{D}^*$ bound state. In conclusion, the repulsive nature of the TPE, which is shared by both T_{cc} and $X(3872)$, is much responsible for their extremely near-threshold phenomena.

ACKNOWLEDGMENTS

We thank Chao Wang for giving the valuable support of the BS equation framework, and thank Zhe Liu for checking the calculations. This work is supported by the National Natural Science Foundation of China under Grant No. 12465016 and No. 12005168, the Natural Science Foundation of Gansu Province (No. 22JR5RA171).

Appendix A: The interaction kernels of the DD^* systems at $O(\epsilon^2)$

Here we list the kernels $\mathcal{K}^{I=0,1}$ at the second order $O(\epsilon^2)$,

$$\begin{aligned} \mathcal{K}_{\text{contact}(2)}^{I=0,\mu\nu} = & im_1 m_2 \frac{g^2}{f^2} \left\{ 6(D_a + D_b - 3E_a - 3E_b) \left[(d-1)\partial_\omega J_{22}^b(-\delta) + (d-2)\partial_\omega J_{22}^b(0) + \partial_\omega J_{22}^b(\delta) \right] + 6(d-2)(d-3) \right. \\ & \times (D_a - D_b + E_a - E_b) J_{22}^g(0,0) + 6 \left[d(D_a - D_b + E_a - E_b) + 2(D_b + E_b) \right] J_{22}^g(-\delta, -\delta) + 12(D_a + E_a) J_{22}^g(\delta, \delta) \\ & \left. + 12(D_b + E_b) J_{22}^g(-\delta, \delta) + 12(D_b + E_b) J_{22}^g(\delta, -\delta) \right\} g^{\mu\nu}, \end{aligned} \quad (\text{A1})$$

$$\begin{aligned} \mathcal{K}_{\text{contact}(2)}^{I=1,\mu\nu} = & im_1 m_2 \frac{g^2}{f^2} \left\{ 6(D_a - D_b + E_a - E_b) \left[(d-1)\partial_\omega J_{22}^b(-\delta) + (d-2)\partial_\omega J_{22}^b(0) + \partial_\omega J_{22}^b(\delta) \right] + 2(d-2)(d-3) \right. \\ & \times (3D_a - D_b - E_a - 5E_b) J_{22}^g(0,0) + 4(d-2)(d-3)(D_b - 3E_b) J_{22}^g(0, -\delta) + 4(d-2)(d-3)(D_b - 3E_b) J_{22}^g(-\delta, 0) \\ & + 2 \left[(3d-2)D_a - (d-2)D_b + (6-d)E_a + (10-5d)E_b \right] J_{22}^g(-\delta, -\delta) + 8(D_a + E_a) J_{22}^g(\delta, \delta) \\ & \left. - 8(D_b + E_b) J_{22}^g(-\delta, \delta) - 8(D_b + E_b) J_{22}^g(\delta, -\delta) \right\} g^{\mu\nu}, \end{aligned} \quad (\text{A2})$$

$$\begin{aligned} \mathcal{K}_{1\pi(2)}^{I=0,\mu\nu} = & im_1 m_2 \frac{1}{p^2 - m^2} \left\{ \frac{g^4}{f^4} \left[\frac{9}{4} \left((d-1)\partial_\omega J_{22}^b(-\delta) + (d-2)\partial_\omega J_{22}^b(0) + \partial_\omega J_{22}^b(\delta) \right) + \frac{3}{4} (d-2)(d-3) J_{22}^g(0, -\delta) \right. \right. \\ & \left. \left. + \frac{3}{4} (d-2)(d-3) J_{22}^g(-\delta, 0) - \frac{3}{4} J_{22}^g(-\delta, \delta) - \frac{3}{4} J_{22}^g(\delta, -\delta) \right] - 6 \frac{g^2}{f^4} J_0^c \right\} p^\mu p^\nu, \end{aligned} \quad (\text{A3})$$

$$\mathcal{K}_{1\pi(2)}^{I=1,\mu\nu} = im_1 m_2 \frac{1}{p^2 - m^2} \left\{ \frac{g^4}{f^4} \left[\frac{3}{4} \left((d-1)\partial_\omega J_{22}^b(-\delta) + (d-2)\partial_\omega J_{22}^b(0) + \partial_\omega J_{22}^b(\delta) \right) + \frac{1}{4} (d-2)(d-3) J_{22}^g(0, -\delta) \right. \right.$$

$$+ \frac{1}{4}(d-2)(d-3)J_{22}^g(-\delta, 0) - \frac{1}{4}J_{22}^g(-\delta, \delta) - \frac{1}{4}J_{22}^g(\delta, -\delta) \left] - 2\frac{g^2}{f^4}J_0^c \right\} p^\mu p^\nu, \quad (\text{A4})$$

$$\mathcal{K}_{2\pi(2)}^{I=0,\mu\nu} = \mathcal{K}_{2\pi(2)}^{I=0,\mu\nu}(q) + \mathcal{K}_{2\pi(2)}^{I=0,\mu\nu}(p), \quad (\text{A5})$$

with

$$\begin{aligned} \mathcal{K}_{2\pi(2)}^{I=0,\mu\nu}(q) = & im_1 m_2 \frac{-3}{4f^4} \left\{ \left[(d-3)J_{22}^R(-\delta, 0)\vec{q}^4 + 2(d-3)J_{32}^R(-\delta, 0)\vec{q}^4 + (d-3)J_{43}^R(-\delta, 0)\vec{q}^4 - (d-3)J_{21}^R(-\delta, 0)\vec{q}^2 \right. \right. \\ & - (2d+1)(d-3)J_{31}^R(-\delta, 0)\vec{q}^2 - J_{31}^R(-\delta, \delta)\vec{q}^2 - (2d+1)(d-3)J_{42}^R(-\delta, 0)\vec{q}^2 - J_{42}^R(-\delta, \delta)\vec{q}^2 \\ & + (d-3)(d-2)(d+1)J_{41}^R(-\delta, 0) + (d+1)J_{41}^R(-\delta, \delta) \left. \right] g^4 + 2 \left[(d-3)q_0 J_{11}^S(0)\vec{q}^2 - q_0 J_{11}^T(-\delta)\vec{q}^2 \right. \\ & + 3(d-3)q_0 J_{22}^S(0)\vec{q}^2 - 3q_0 J_{22}^T(-\delta)\vec{q}^2 + 2(d-3)J_{24}^S(0)\vec{q}^2 - 2J_{24}^T(-\delta)\vec{q}^2 + 2(d-3)q_0 J_{32}^S(0)\vec{q}^2 - 2q_0 J_{32}^T(-\delta)\vec{q}^2 \\ & + 2(d-3)J_{33}^S(0)\vec{q}^2 - 2J_{33}^T(-\delta)\vec{q}^2 - (d-3)(d-2)q_0 J_{21}^S(0) - q_0 J_{21}^S(\delta) + (d-1)q_0 J_{21}^T(-\delta) \\ & - 2(d-3)(d-2)q_0 J_{31}^S(0) - 2q_0 J_{31}^S(\delta) + 2(d-1)q_0 J_{31}^T(-\delta) - 2(d-3)(d-2)J_{34}^S(0) - 2J_{34}^S(\delta) + 2(d-1)J_{34}^T(-\delta) \left. \right] g^2 \\ & + q_0^2 J_0^F + 4q_0^2 J_{11}^F + 4q_0^2 J_{21}^F + 4J_{22}^F \left. \right\} g^{\mu\nu} + im_1 m_2 \frac{-3g^2}{2f^4} \left\{ \frac{-1}{2} \left[- (d-3)J_{22}^R(-\delta, 0)\vec{q}^2 + J_{22}^R(-\delta, \delta)\vec{q}^2 \right. \right. \\ & - 2(d-3)J_{32}^R(-\delta, 0)\vec{q}^2 + 2J_{32}^R(-\delta, \delta)\vec{q}^2 - (d-3)J_{43}^R(-\delta, 0)\vec{q}^2 + J_{43}^R(-\delta, \delta)\vec{q}^2 + (d-3)J_{21}^R(-\delta, 0) - J_{21}^R(-\delta, \delta) \\ & + (d^2-9)J_{31}^R(-\delta, 0) - (d+3)J_{31}^R(-\delta, \delta) + (d^2-9)J_{42}^R(-\delta, 0) - (d+3)J_{42}^R(-\delta, \delta) \left. \right] g^2 + (d-3)q_0 J_{11}^S(0) - q_0 J_{11}^S(\delta) \\ & + 3(d-3)q_0 J_{22}^S(0) - 3q_0 J_{22}^S(\delta) + 2(d-3)J_{24}^S(0) - 2J_{24}^S(\delta) + 2(d-3)q_0 J_{32}^S(0) - 2q_0 J_{32}^S(\delta) + 2(d-3)J_{33}^S(0) \\ & \left. - 2J_{33}^S(\delta) \right\} q^\mu q^\nu, \quad (\text{A6}) \end{aligned}$$

$$\mathcal{K}_{2\pi(2)}^{I=0,\mu\nu}(p) = im_1 m_2 \frac{-3(d-3)g^4}{4f^4} J_{21}^R(-\delta, -\delta) \left[\vec{p}^2 g^{\mu\nu} + p^\mu p^\nu \right], \quad (\text{A7})$$

$$\mathcal{K}_{2\pi(2)}^{I=1,\mu\nu} = \mathcal{K}_{2\pi(2)}^{I=1,\mu\nu}(q) + \mathcal{K}_{2\pi(2)}^{I=1,\mu\nu}(p), \quad (\text{A8})$$

with

$$\begin{aligned} \mathcal{K}_{2\pi(2)}^{I=1,\mu\nu}(q) = & im_1 m_2 \frac{1}{4f^4} \left\{ (-5) \left[- (d-3)J_{22}^R(-\delta, 0)\vec{q}^4 - 2(d-3)J_{32}^R(-\delta, 0)\vec{q}^4 - (d-3)J_{43}^R(-\delta, 0)\vec{q}^4 + (d-3)J_{21}^R(-\delta, 0)\vec{q}^2 \right. \right. \\ & + (d-3)(2d+1)J_{31}^R(-\delta, 0)\vec{q}^2 + J_{31}^R(-\delta, \delta)\vec{q}^2 + (d-3)(2d+1)J_{42}^R(-\delta, 0)\vec{q}^2 + J_{42}^R(-\delta, \delta)\vec{q}^2 \\ & - (d-3)(d-2)(d+1)J_{41}^R(-\delta, 0) - (d+1)J_{41}^R(-\delta, \delta) \left. \right] g^4 + 2 \left[(d-3)q_0 J_{11}^S(0)\vec{q}^2 - q_0 J_{11}^T(-\delta)\vec{q}^2 + 3(d-3)q_0 J_{22}^S(0)\vec{q}^2 \right. \\ & - 3q_0 J_{22}^T(-\delta)\vec{q}^2 + 2(d-3)J_{24}^S(0)\vec{q}^2 - 2J_{24}^T(-\delta)\vec{q}^2 + 2(d-3)q_0 J_{32}^S(0)\vec{q}^2 - 2q_0 J_{32}^T(-\delta)\vec{q}^2 + 2(d-3)J_{33}^S(0)\vec{q}^2 \\ & - 2J_{33}^T(-\delta)\vec{q}^2 - (d-3)(d-2)q_0 J_{21}^S(0) - q_0 J_{21}^S(\delta) + (d-1)q_0 J_{21}^T(-\delta) - 2(d-3)(d-2)q_0 J_{31}^S(0) - 2q_0 J_{31}^S(\delta) \\ & + 2(d-1)q_0 J_{31}^T(-\delta) - 2(d-3)(d-2)J_{34}^S(0) - 2J_{34}^S(\delta) + 2(d-1)J_{34}^T(-\delta) \left. \right] g^2 + q_0^2 J_0^F + 4q_0^2 J_{11}^F + 4q_0^2 J_{21}^F + 4J_{22}^F \left. \right\} g^{\mu\nu} \\ & + im_1 m_2 \frac{g^2}{2f^4} \left\{ \frac{-5}{2} \left[- (d-3)J_{22}^R(-\delta, 0)\vec{q}^2 + J_{22}^R(-\delta, \delta)\vec{q}^2 - 2(d-3)J_{32}^R(-\delta, 0)\vec{q}^2 + 2J_{32}^R(-\delta, \delta)\vec{q}^2 \right. \right. \\ & - (d-3)J_{43}^R(-\delta, 0)\vec{q}^2 + J_{43}^R(-\delta, \delta)\vec{q}^2 + (d-3)J_{21}^R(-\delta, 0) - J_{21}^R(-\delta, \delta) + (d^2-9)J_{31}^R(-\delta, 0) - (d-3)J_{31}^R(-\delta, \delta) \\ & + (d^2-9)J_{42}^R(-\delta, 0) - (d+3)J_{42}^R(-\delta, \delta) \left. \right] g^2 + (d-3)q_0 J_{11}^S(0) - q_0 J_{11}^S(\delta) + 3(d-3)q_0 J_{22}^S(0) - 3q_0 J_{22}^S(\delta) \\ & + 2(d-3)J_{24}^S(0) - 2J_{24}^S(\delta) + 2(d-3)q_0 J_{32}^S(0) - 2q_0 J_{32}^S(\delta) + 2(d-3)J_{33}^S(0) - 2J_{33}^S(\delta) \left. \right\} q^\mu q^\nu, \quad (\text{A9}) \end{aligned}$$

$$\mathcal{K}_{2\pi(2)}^{I=1,\mu\nu}(p) = im_1 m_2 \frac{-5(d-3)g^4}{4f^4} J_{21}^R(-\delta, -\delta) \left[\vec{p}^2 g^{\mu\nu} + p^\mu p^\nu \right]. \quad (\text{A10})$$

- [2] Y.-R. Liu, X. Liu, W.-Z. Deng, and S.-L. Zhu, Is $X(3872)$ Really a Molecular State?, *Eur. Phys. J.* **C56**, 63 (2008), [arXiv:0801.3540 \[hep-ph\]](#).
- [3] H.-X. Chen, W. Chen, X. Liu, and S.-L. Zhu, The hidden-charm pentaquark and tetraquark states, *Phys. Rept.* **639**, 1 (2016), [arXiv:1601.02092 \[hep-ph\]](#).
- [4] M. T. AlFiky, F. Gabbiani, and A. A. Petrov, $X(3872)$: Hadronic molecules in effective field theory, *Phys. Lett.* **B640**, 238 (2006), [arXiv:hep-ph/0506141 \[hep-ph\]](#).
- [5] F.-K. Guo, C. Hanhart, U.-G. Meissner, Q. Wang, Q. Zhao, and B.-S. Zou, Hadronic molecules, *Rev. Mod. Phys.* **90**, 015004 (2018), [arXiv:1705.00141 \[hep-ph\]](#).
- [6] X.-K. Dong, F.-K. Guo, and B.-S. Zou, A survey of heavy-antiheavy hadronic molecules, *Progr. Phys.* **41**, 65 (2021), [arXiv:2101.01021 \[hep-ph\]](#).
- [7] X.-K. Dong, F.-K. Guo, and B.-S. Zou, A survey of heavy-heavy hadronic molecules, *Commun. Theor. Phys.* **73**, 125201 (2021), [arXiv:2108.02673 \[hep-ph\]](#).
- [8] M.-Z. Liu, Y.-W. Pan, Z.-W. Liu, T.-W. Wu, J.-X. Lu, and L.-S. Geng, Three ways to decipher the nature of exotic hadrons: Multiplets, three-body hadronic molecules, and correlation functions, *Phys. Rept.* **1108**, 1 (2025), [arXiv:2404.06399 \[hep-ph\]](#).
- [9] E. S. Swanson, Short range structure in the $X(3872)$, *Phys. Lett. B* **588**, 189 (2004), [arXiv:hep-ph/0311229](#).
- [10] G. Yang, J. Ping, and J. Segovia, Tetra- and pentaquark structures in the constituent quark model, *Symmetry* **12**, 1869 (2020), [arXiv:2009.00238 \[hep-ph\]](#).
- [11] P. G. Ortega and D. R. Entem, Coupling hadron-hadron thresholds within a chiral quark model approach, *Symmetry* **13**, 279 (2021), [arXiv:2012.10105 \[hep-ph\]](#).
- [12] H. Huang, C. Deng, X. Liu, Y. Tan, and J. Ping, Tetraquarks and Pentaquarks from Quark Model Perspective, *Symmetry* **15**, 1298 (2023).
- [13] M. Mai, U.-G. Meißner, and C. Urbach, Towards a theory of hadron resonances, *Phys. Rept.* **1001**, 1 (2023), [arXiv:2206.01477 \[hep-ph\]](#).
- [14] P. Bicudo, Tetraquarks and pentaquarks in lattice QCD with light and heavy quarks, *Phys. Rept.* **1039**, 1 (2023), [arXiv:2212.07793 \[hep-lat\]](#).
- [15] A. Esposito, A. Pilloni, and A. D. Polosa, Multi-quark Resonances, *Phys. Rept.* **668**, 1 (2017), [arXiv:1611.07920 \[hep-ph\]](#).
- [16] A. Ali, J. S. Lange, and S. Stone, Exotics: Heavy Pentaquarks and Tetraquarks, *Prog. Part. Nucl. Phys.* **97**, 123 (2017), [arXiv:1706.00610 \[hep-ph\]](#).
- [17] R. F. Lebed, R. E. Mitchell, and E. S. Swanson, Heavy-Quark QCD Exotica, *Prog. Part. Nucl. Phys.* **93**, 143 (2017), [arXiv:1610.04528 \[hep-ph\]](#).
- [18] N. Brambilla, S. Eidelman, C. Hanhart, A. Nefediev, C.-P. Shen, C. E. Thomas, A. Vairo, and C.-Z. Yuan, The XYZ states: experimental and theoretical status and perspectives, *Phys. Rept.* **873**, 1 (2020), [arXiv:1907.07583 \[hep-ex\]](#).
- [19] Y.-R. Liu, H.-X. Chen, W. Chen, X. Liu, and S.-L. Zhu, Pentaquark and Tetraquark states, *Prog. Part. Nucl. Phys.* **107**, 237 (2019), [arXiv:1903.11976 \[hep-ph\]](#).
- [20] W. Lucha, D. Melikhov, and H. Sazdjian, Tetraquarks in large- N_c QCD, *Prog. Part. Nucl. Phys.* **120**, 103867 (2021), [arXiv:2102.02542 \[hep-ph\]](#).
- [21] H.-X. Chen, W. Chen, X. Liu, Y.-R. Liu, and S.-L. Zhu, An updated review of the new hadron states, *Rept. Prog. Phys.* **86**, 026201 (2023), [arXiv:2204.02649 \[hep-ph\]](#).
- [22] A. Hosaka, T. Iijima, K. Miyabayashi, Y. Sakai, and S. Yasui, Exotic hadrons with heavy flavors: X , Y , Z , and related states, *PTEP* **2016**, 062C01 (2016), [arXiv:1603.09229 \[hep-ph\]](#).
- [23] S. Weinberg, Nuclear forces from chiral Lagrangians, *Phys. Lett.* **B251**, 288 (1990).
- [24] S. Weinberg, Effective chiral Lagrangians for nucleon - pion interactions and nuclear forces, *Nucl. Phys.* **B363**, 3 (1991).
- [25] E. Epelbaum, H.-W. Hammer, and U.-G. Meissner, Modern Theory of Nuclear Forces, *Rev. Mod. Phys.* **81**, 1773 (2009), [arXiv:0811.1338 \[nucl-th\]](#).
- [26] U.-G. Meißner, A new tool in nuclear physics: Nuclear lattice simulations, *Nucl. Phys. News.* **24**, 11 (2014), [arXiv:1505.06997 \[nucl-th\]](#).
- [27] R. Machleidt and F. Sammarruca, Chiral EFT based nuclear forces: Achievements and challenges, *Phys. Scripta* **91**, 083007 (2016), [arXiv:1608.05978 \[nucl-th\]](#).
- [28] U.-G. Meissner, The long and winding road from chiral effective Lagrangians to nuclear structure, *Phys. Scripta* **91**, 033005 (2016), [arXiv:1510.03230 \[nucl-th\]](#).
- [29] E. Epelbaum, H. Krebs, and P. Reinert, High-precision nuclear forces from chiral EFT: State-of-the-art, challenges and outlook, *Front. in Phys.* **8**, 98 (2020), [arXiv:1911.11875 \[nucl-th\]](#).
- [30] H. W. Hammer, S. König, and U. van Kolck, Nuclear effective field theory: status and perspectives, *Rev. Mod. Phys.* **92**, 025004 (2020), [arXiv:1906.12122 \[nucl-th\]](#).
- [31] L. Meng, B. Wang, G.-J. Wang, and S.-L. Zhu, Chiral perturbation theory for heavy hadrons and chiral effective field theory for heavy hadronic molecules, *Phys. Rept.* **1019**, 1 (2023), [arXiv:2204.08716 \[hep-ph\]](#).
- [32] S. Scherer and M. R. Schindler, A Primer for Chiral Perturbation Theory, Springer-Verlag, Berlin **Vol. 830**, p. 1 (2012).
- [33] Z.-W. Liu, N. Li, and S.-L. Zhu, Chiral perturbation theory and the $\bar{B}\bar{B}$ strong interaction, *Phys. Rev.* **D89**, 074015 (2014), [arXiv:1211.3578 \[hep-ph\]](#).
- [34] H. Xu, B. Wang, Z.-W. Liu, and X. Liu, DD^* potentials in chiral perturbation theory and possible molecular states, *Phys. Rev. D* **99**, 014027 (2019), [Erratum: *Phys.Rev.D* 104, 119903 (2021)], [arXiv:1708.06918 \[hep-ph\]](#).
- [35] Z. Liu, H. Xu, and X. Liu, $D^{(*)}\bar{B}^{(*)}$ dynamics in chiral effective field theory, *Phys. Rev. D* **112**, 034007 (2025), [arXiv:2503.10299 \[hep-ph\]](#).
- [36] B. Wang, Z.-W. Liu, and X. Liu, $\bar{B}^{(*)}\bar{B}^{(*)}$ interactions in chiral effective field theory, *Phys. Rev. D* **99**, 036007 (2019), [arXiv:1812.04457 \[hep-ph\]](#).
- [37] L. Meng, B. Wang, G.-J. Wang, and S.-L. Zhu, The hidden charm pentaquark states and $\Sigma_c\bar{D}^{(*)}$ interaction in chiral perturbation theory, *Phys. Rev. D* **100**, 014031 (2019), [arXiv:1905.04113 \[hep-ph\]](#).
- [38] B. Wang, L. Meng, and S.-L. Zhu, Spectrum of the strange hidden charm molecular pentaquarks in chiral effective field theory, *Phys. Rev. D* **101**, 034018 (2020), [arXiv:1912.12592 \[hep-ph\]](#).
- [39] B. Wang, L. Meng, and S.-L. Zhu, Hidden-charm and hidden-bottom molecular pentaquarks in chiral effective field theory, *JHEP* **11**, 108, [arXiv:1909.13054 \[hep-ph\]](#).
- [40] L. Meng, B. Wang, and S.-L. Zhu, $\Sigma_c N$ interaction in chiral effective field theory, *Phys. Rev. C* **101**, 064002 (2020), [arXiv:1912.09661 \[nucl-th\]](#).
- [41] B. Wang, L. Meng, and S.-L. Zhu, $D^{(*)}N$ interaction and the structure of $\Sigma_c(2800)$ and $\Lambda_c(2940)$ in chiral effective field theory, *Phys. Rev. D* **101**, 094035 (2020), [arXiv:2003.05688 \[hep-ph\]](#).

- [42] K. Chen, B. Wang, and S.-L. Zhu, Exploration of the doubly charmed molecular pentaquarks, *Phys. Rev. D* **103**, 116017 (2021), arXiv:2102.05868 [hep-ph].
- [43] K. Chen, B.-L. Huang, B. Wang, and S.-L. Zhu, $\Sigma_c \Sigma_c$ interactions in chiral effective field theory, (2022), arXiv:2204.13316 [hep-ph].
- [44] Z.-L. Zhang, Z.-W. Liu, S.-Q. Luo, F.-L. Wang, B. Wang, and H. Xu, $\Lambda_c(2910)$ and $\Lambda_c(2940)$ as conventional baryons dressed with the D^*N channel, *Phys. Rev. D* **107**, 034036 (2023), arXiv:2210.17188 [hep-ph].
- [45] B.-L. Huang, B. Wang, and S.-L. Zhu, Octet baryon and heavy meson interactions in chiral effective field theory, *Phys. Rev. D* **110**, 116007 (2024), arXiv:2402.00460 [hep-ph].
- [46] R. Aaij et al. (LHCb collaboration), Observation of an exotic narrow doubly charmed tetraquark, *Nature Phys.* **18**, 751 (2022), arXiv:2109.01038 [hep-ex].
- [47] R. Aaij et al. (LHCb collaboration), Study of the doubly charmed tetraquark T_{cc}^+ , *Nature Commun.* **13**, 3351 (2022), arXiv:2109.01056 [hep-ex].
- [48] Z.-M. Ding, H.-Y. Jiang, and J. He, Molecular states from $D^{(*)}\bar{D}^{(*)}/B^{(*)}\bar{B}^{(*)}$ and $D^{(*)}D^{(*)}/\bar{B}^{(*)}\bar{B}^{(*)}$ interactions, *Eur. Phys. J. C* **80**, 1179 (2020), arXiv:2011.04980 [hep-ph].
- [49] L. Meng, G.-J. Wang, B. Wang, and S.-L. Zhu, Probing the long-range structure of the T_{cc}^+ with the strong and electromagnetic decays, *Phys. Rev. D* **104**, 051502 (2021), arXiv:2107.14784 [hep-ph].
- [50] R. Chen, Q. Huang, X. Liu, and S.-L. Zhu, Predicting another doubly charmed molecular resonance T_{cc}^+ (3876), *Phys. Rev. D* **104**, 114042 (2021), arXiv:2108.01911 [hep-ph].
- [51] M.-J. Yan and M. P. Valderrama, Subleading contributions to the decay width of the T_{cc}^+ tetraquark, *Phys. Rev. D* **105**, 014007 (2022), arXiv:2108.04785 [hep-ph].
- [52] M.-J. Zhao, Z.-Y. Wang, C. Wang, and X.-H. Guo, Investigation of the possible $DD^*/B\bar{B}^*$ and $DD^*/\bar{B}\bar{B}^*$ bound states, *Phys. Rev. D* **105**, 096016 (2022), arXiv:2112.12633 [hep-ph].
- [53] F.-L. Wang and X. Liu, Investigating new type of doubly charmed molecular tetraquarks composed of charmed mesons in the H and T doublets, *Phys. Rev. D* **104**, 094030 (2021), arXiv:2108.09925 [hep-ph].
- [54] J.-B. Cheng, Z.-Y. Lin, and S.-L. Zhu, Double-charm tetraquark under the complex scaling method, *Phys. Rev. D* **106**, 016012 (2022), arXiv:2205.13354 [hep-ph].
- [55] Z.-Y. Lin, J.-B. Cheng, and S.-L. Zhu, T_{cc}^+ and χ_{c1} (3872) with the complex scaling method and $DD(\bar{D})\pi$ three-body effect, *Phys. Rev. D* **110**, 054008 (2024), arXiv:2205.14628 [hep-ph].
- [56] L. M. Abreu, A note on the possible bound $D^{(*)}D^{(*)}$, $\bar{B}^{(*)}\bar{B}^{(*)}$ and $D^{(*)}\bar{B}^{(*)}$ states, *Nucl. Phys. B* **985**, 115994 (2022), arXiv:2206.01166 [hep-ph].
- [57] Z.-F. Sun, N. Li, and X. Liu, Isospin violation effect and three-body decays of the T_{cc}^+ state, *Phys. Rev. D* **110**, 094025 (2024), arXiv:2405.00525 [hep-ph].
- [58] J.-B. Cheng, S.-Y. Li, Y.-R. Liu, Z.-G. Si, and T. Yao, Double-heavy tetraquark states with heavy diquark-antiquark symmetry, *Chin. Phys. C* **45**, 043102 (2021), arXiv:2008.00737 [hep-ph].
- [59] X.-Z. Weng, W.-Z. Deng, and S.-L. Zhu, Doubly heavy tetraquarks in an extended chromomagnetic model, *Chin. Phys. C* **46**, 013102 (2022), arXiv:2108.07242 [hep-ph].
- [60] T. Guo, J. Li, J. Zhao, and L. He, Mass spectra of doubly heavy tetraquarks in an improved chromomagnetic interaction model, *Phys. Rev. D* **105**, 014021 (2022), arXiv:2108.10462 [hep-ph].
- [61] K. Chen, R. Chen, L. Meng, B. Wang, and S.-L. Zhu, Systematics of the heavy flavor hadronic molecules, *Eur. Phys. J. C* **82**, 581 (2022), arXiv:2109.13057 [hep-ph].
- [62] X.-Y. Liu, W.-X. Zhang, and D. Jia, Doubly heavy tetraquarks: Heavy quark bindings and chromomagnetically mixings, *Phys. Rev. D* **108**, 054019 (2023), arXiv:2303.03923 [hep-ph].
- [63] Y. Ma, L. Meng, Y.-K. Chen, and S.-L. Zhu, Doubly heavy tetraquark states in the constituent quark model using diffusion Monte Carlo method, *Phys. Rev. D* **109**, 074001 (2024), arXiv:2309.17068 [hep-ph].
- [64] W.-L. Wu, Y. Ma, Y.-K. Chen, L. Meng, and S.-L. Zhu, Doubly heavy tetraquark bound and resonant states, *Phys. Rev. D* **110**, 094041 (2024), arXiv:2409.03373 [hep-ph].
- [65] M. Padmanath and S. Prelovsek, Signature of a Doubly Charm Tetraquark Pole in DD^* Scattering on the Lattice, *Phys. Rev. Lett.* **129**, 032002 (2022), arXiv:2202.10110 [hep-lat].
- [66] Y. Lyu, S. Aoki, T. Doi, T. Hatsuda, Y. Ikeda, and J. Meng, Doubly Charmed Tetraquark T_{cc}^+ from Lattice QCD near Physical Point, *Phys. Rev. Lett.* **131**, 161901 (2023), arXiv:2302.04505 [hep-lat].
- [67] L. Meng, V. Baru, E. Epelbaum, A. A. Filin, and A. M. Gasparyan, Solving the left-hand cut problem in lattice QCD: T_{cc}^+ (3875) from finite volume energy levels, *Phys. Rev. D* **109**, L071506 (2024), arXiv:2312.01930 [hep-lat].
- [68] L. Meng, E. Ortiz-Pacheco, V. Baru, E. Epelbaum, M. Padmanath, and S. Prelovsek, Doubly charm tetraquark channel with isospin 1 from lattice QCD, *Phys. Rev. D* **111**, 034509 (2025), arXiv:2411.06266 [hep-lat].
- [69] S. Collins, A. Nefediev, M. Padmanath, and S. Prelovsek, Toward the quark mass dependence of T_{cc}^+ from lattice QCD, *Phys. Rev. D* **109**, 094509 (2024), arXiv:2402.14715 [hep-lat].
- [70] A. Francis, Lattice perspectives on doubly heavy tetraquarks, *Prog. Part. Nucl. Phys.* **140**, 104143 (2025), arXiv:2502.04701 [hep-lat].
- [71] S. M. Dawid, F. Romero-López, and S. R. Sharpe, Finite- and infinite-volume study of $DD\pi$ scattering, *JHEP* **01**, 060, arXiv:2409.17059 [hep-lat].
- [72] F. Gil-Domínguez, A. Giachino, and R. Molina, Quark mass dependence of the T_{cc}^+ (3875) pole, *Phys. Rev. D* **111**, 016029 (2025), arXiv:2409.15141 [hep-ph].
- [73] T. Whyte, D. J. Wilson, and C. E. Thomas (Hadron Spectrum), Near-threshold states in coupled $DD^*-D^*D^*$ scattering from lattice QCD, *Phys. Rev. D* **111**, 034511 (2025), arXiv:2405.15741 [hep-lat].
- [74] S. Prelovsek, E. Ortiz-Pacheco, S. Collins, L. Leskovec, M. Padmanath, and I. Vujmilovic, Doubly heavy tetraquarks from lattice QCD: Incorporating diquark-antidiquark operators and the left-hand cut, *Phys. Rev. D* **112**, 014507 (2025), arXiv:2504.03473 [hep-lat].
- [75] N. Pitanga Lachini, C. E. Thomas, and D. J. Wilson, Coupled-channel scattering of DD , DD^* and D^*D^* in isospin-1 from lattice QCD, (2025), arXiv:2505.01363 [hep-lat].
- [76] Y. Li, Y.-B. He, X.-H. Liu, B. Chen, and H.-W. Ke, Searching for doubly charmed tetraquark candidates T_{cc} and $T_{cc\bar{s}}$ in B_c decays, *Eur. Phys. J. C* **83**, 258 (2023), arXiv:2302.02518 [hep-ph].
- [77] B. Chen, M. Yang, G. Chen, J. Zhao, and X.-h. Liu, Production of doubly charmed hadrons Ξ_{cc}^{++} and T_{cc}^+ in relativistic heavy-ion collisions, *Phys. Rev. C* **109**, 064909 (2024), arXiv:2309.02987 [nucl-th].
- [78] X.-L. Hua, Y.-Y. Li, Q. Wang, S. Yang, Q. Zhao, and B.-S. Zou, Revealing the mystery of the double charm tetraquark in pp collision, *Eur. Phys. J. C* **84**, 800 (2024), arXiv:2310.04258 [hep-ph].
- [79] E. Y. Paryev, An alternative way to decipher the na-

- ture of the doubly charmed tetraquark $T_{cc}^+(3875)$: Its antiparticle $T_{\bar{c}\bar{c}}^-(3875)$ photoproduction off nuclei near threshold, [Int. J. Mod. Phys. A **39**, 2450115 \(2024\)](#), [arXiv:2408.00360 \[hep-ph\]](#).
- [80] B. Wang and L. Meng, Revisiting the DD^* chiral interactions with the local momentum-space regularization up to the third order and the nature of T_{cc}^+ , [Phys. Rev. D **107**, 094002 \(2023\)](#), [arXiv:2212.08447 \[hep-ph\]](#).
- [81] Q.-Y. Zhai, M.-Z. Liu, J.-X. Lu, and L.-S. Geng, Long-range S-wave DD^* interaction in covariant chiral effective field theory, [Phys. Rev. D **109**, 034015 \(2024\)](#), [arXiv:2311.06569 \[hep-ph\]](#).
- [82] J. T. Chacko, V. Baru, C. Hanhart, and S. L. Krug, Two-pion exchange for coupled-channel scattering of two heavy mesons, [Phys. Rev. D **111**, 034042 \(2025\)](#), [arXiv:2411.13303 \[hep-ph\]](#).
- [83] G. Burdman and J. F. Donoghue, Union of chiral and heavy quark symmetries, [Phys. Lett. **B280**, 287 \(1992\)](#).
- [84] M. B. Wise, Chiral perturbation theory for hadrons containing a heavy quark, [Phys. Rev. **D45**, R2188 \(1992\)](#).
- [85] T.-M. Yan, H.-Y. Cheng, C.-Y. Cheung, G.-L. Lin, Y. C. Lin, and H.-L. Yu, Heavy quark symmetry and chiral dynamics, [Phys. Rev. **D46**, 1148 \(1992\)](#), [Erratum: [Phys. Rev. **D55**, 5851 \(1997\)](#)].
- [86] M. P. Valderrama, Power Counting and Perturbative One Pion Exchange in Heavy Meson Molecules, [Phys. Rev. **D85**, 114037 \(2012\)](#), [arXiv:1204.2400 \[hep-ph\]](#).